THE JOURNAL OF BIOLOGICAL CHEMISTRY VOL. 290, NO. 10, pp. 6531–6545, March 6, 2015

Aldo-keto Reductase 1B15 (AKR1B15)

*A MITOCHONDRIAL HUMAN ALDO-KETO REDUCTASE WITH ACTIVITY TOWARD STEROIDS AND 3-KETO-ACYL-CoA CONJUGATES**

Received for publication, September 9, 2014, and in revised form, January 8, 2015 Published, JBC Papers in Press, January 10, 2015, DOI 10.1074/jbc.M114.610121

Susanne Weber[‡], Joshua K. Salabei[§], Gabriele Möller[‡], Elisabeth Kremmer[¶], Aruni Bhatnagar[§], Jerzy Adamski[‡‖1], and Oleg A. Barski[§2]**

*From the [‡]Helmholtz Zentrum Muenchen, German Research Center for Environmental Health, Institute of Experimental Genetics, Genome Analysis Center, 85764 Neuherberg, Germany, the [§]Diabetes and Obesity Center, School of Medicine, University of Louisville, Louisville, Kentucky 40202, the [¶]Institute of Molecular Immunology, German Research Center for Environmental Health, Helmholtz Zentrum Muenchen, 81377 Muenchen, Germany, the [‖]Lehrstuhl für Experimentelle Genetik, Technische Universitaet Muenchen, 85356 Freising-Weihenstephan, Germany, and the **German Center for Diabetes Research, 85764 Neuherberg, Germany*

Background: Aldo-keto reductases (AKRs) are enzymes involved in the metabolism of carbonyl substrates.
Results: Two alternatively spliced protein isoforms encoded by the human AKR gene *AKR1B15* were identified. The AKR1B15.1 isoform catalyzes reduction of steroids and 3-keto-acyl-CoA conjugates and localizes to mitochondria.
Conclusion: AKR1B15.1 is a mitochondrial carbonyl reductase.
Significance: AKR1B15.1 is a new enzyme with unique localization and catalytic features.

Aldo-keto reductases (AKRs) comprise a superfamily of proteins involved in the reduction and oxidation of biogenic and xenobiotic carbonyls. In humans, at least 15 AKR superfamily members have been identified so far. One of these is a newly identified gene locus, *AKR1B15*, which clusters on chromosome 7 with the other human *AKR1B* subfamily members (*i.e. AKR1B1* and *AKR1B10*). We show that alternative splicing of the *AKR1B15* gene transcript gives rise to two protein isoforms with different N termini: AKR1B15.1 is a 316-amino acid protein with 91% amino acid identity to AKR1B10; AKR1B15.2 has a prolonged N terminus and consists of 344 amino acid residues. The two gene products differ in their expression level, subcellular localization, and activity. In contrast with other AKR enzymes, which are mostly cytosolic, AKR1B15.1 co-localizes with the mitochondria. Kinetic studies show that AKR1B15.1 is predominantly a reductive enzyme that catalyzes the reduction of androgens and estrogens with high positional selectivity (17β-hydroxysteroid dehydrogenase activity) as well as 3-keto-acyl-CoA conjugates and exhibits strong cofactor selectivity toward NADP(H). In accordance with its substrate spectrum, the enzyme is expressed at the highest levels in steroid-sensitive tissues, namely placenta, testis, and adipose tissue. Placental and adipose expression could be reproduced in the BeWo and SGBS cell lines, respectively. In contrast, AKR1B15.2 localizes to the cytosol and displays no enzymatic activity with the substrates tested. Collectively, these results demonstrate the existence of a novel catalytically active AKR, which is associated with mitochondria and expressed mainly in steroid-sensitive tissues.

The aldo-keto reductase (AKR)[3] superfamily comprises 15 families containing over 150 members that are present in all phyla (1, 2). AKRs are multifunctional enzymes that catalyze the reduction of biogenic and xenobiotic aldehydes and ketones as well as the synthesis and metabolism of sex hormones. The majority of AKRs catalyze oxidation-reduction reactions between carbonyl and alcohol groups, whereas enzymes of the AKR1D family reduce double bonds in the bile acid biosynthesis pathway, acting as 5β-reductases (3). Some AKR proteins have very low or no activity and perform predominantly non-catalytic functions (*e.g.* structural (lens ρ-crystallines: AKR1C10a and AKR1C10b) or regulatory and chaperone-like (voltage-gated potassium channel β-subunits of the AKR6 family: Kvβ) functions) (4, 5).

Prior to identification of AKR1B15, 14 human AKRs have been described. These proteins are generally cytosolic and monomeric with molecular masses ranging between 35 and 40 kDa. These enzymes catalyze oxidation-reduction reactions in a variety of cellular pathways, such as glucose metabolism (AKR1B1) (2), vitamin C biosynthesis (AKR1A1) (6), steroid and prostaglandin metabolism (AKR1Bs and AKR1Cs) (7, 8), bile acid synthesis (AKR1D1) (9), and neurotransmitter metabolism (AKR7) (10), as well as the detoxification of both endogenous oxidation by-products, such as advanced glycation end product precursors or lipid peroxidation-derived aldehydes (11, 12), and exogenous toxins, such as aflatoxin B1 (13) or tobacco-derived carcinogen 4-methyl-nitrosamino-1-(3-pyri-

* This work was supported, in whole or in part, by National Institutes of Health Grants HL55477, HL59378, and GM103492.

[1] To whom correspondence may be addressed: Helmholtz Zentrum Muenchen, German Research Center for Environmental Health, Institute of Experimental Genetics, Genome Analysis Center, Ingolstaedter Landstr. 1, 85764 Neuherberg, Germany. Tel.: 49-89-3187-3155; Fax: 49-89-3187-3225; E-mail: Adamski@helmholtz-muenchen.de.

[2] To whom correspondence may be addressed: Diabetes and Obesity Center, School of Medicine, University of Louisville, 580 S. Preston St., Rm. 421, Louisville, KY 40202. Fax: 502-852-3663; E-mail: olegbarski@gmail.com.

[3] The abbreviations used are: AKR, aldo-keto reductase; AN, androsterone; HSD, hydroxysteroid dehydrogenase; TES, 2-{[2-hydroxy-1,1-bis(hydroxymethyl)ethyl]amino}ethanesulfonic acid; qPCR, quantitative PCR.

dyl)-1-butanone (NNK) (14). Generally, the enzymes of the AKR superfamily prefer NADPH over NADH as a reducing cofactor (2, 15, 16).

The AKR1 family is the most numerous and has been further divided into five subfamilies (A–E). The AKR1B subfamily has been intensely studied due to the potential role of its founding member human aldose reductase (AKR1B1) in the development of diabetic complications (17, 18). Under hyperglycemic conditions, AKR1B1 converts excess glucose into sorbitol, leading to osmotic and redox imbalances and resulting in tissue injury associated with diabetes (19–21). Inhibition of AKR1B1 has been shown to prevent, delay, or reverse tissue injury due to hyperglycemia (19, 22). In this context, a large number of studies and clinical trials have been devoted to finding efficient inhibitors of aldose reductase to prevent the development of diabetic complications; however, these efforts have met with limited success due to problems in trials design, low efficacy, and nonspecific side effects of inhibitors (17, 23). In addition to glucose, AKR1B1 catalyzes the reduction of several substrates of physiological significance, including advanced glycation end-product precursors, 4-hydroxy-*trans*-2-nonenal, and oxidized phospholipids (11, 24, 25), and has been suggested to play important roles in the development of atherosclerosis (26), ischemic preconditioning (27), and restenosis (28).

AKR1B1 is closely related to the small intestine aldose reductase (AKR1B10) (29, 30). In contrast to *AKR1B1*, *AKR1B10* is expressed mainly in small intestine, colon, liver, thymus (29), and adrenal gland (30). AKR1B10 shares 71% amino acid sequence identity with AKR1B1 and exhibits substrate specificity similar to aldose reductase with the exception that it has significantly higher catalytic efficiency with all-*trans*-retinal (31). *AKR1B10* is strongly overexpressed in lung and hepatic carcinomas (squamous cell and adeno-carcinomas) (29) as well as in colorectal and uterine cancers (32) and has been implicated in conferring resistance to anticancer drugs (33, 34).

Recently, a novel gene, *AKR1B15*, with 91% identity to *AKR1B10* has been predicted in the genetic cluster encompassing *AKR1B1* and *AKR1B10* on human chromosome 7. We previously reported that this gene encodes a functional protein (35). However, in contrast to AKR1B1 and AKR1B10, the enzymatic activity of this newly identified AKR was low, and the protein expressed with an N-terminal His tag was found in the microsomal fraction in both the mammalian and bacterial expression systems (35). Although orthologs of AKR1B1 are known in rodents (AKR1B3 in mouse and AKR1B4 in rat), direct orthology between AKR1B15 and AKR1B10 and rodent AKR1Bs has not been established so far.

In the present study, we show that the *AKR1B15* gene gives rise to two alternatively spliced mRNA products, each coding for a unique protein, hereafter referred to as AKR1B15.1 and AKR1B15.2. Furthermore, we characterize the catalytic activity, tissue distribution, and subcellular localization of both AKR1B15 isoforms.

EXPERIMENTAL PROCEDURES

Chemicals and Materials—Primers were synthesized by Integrated DNA Technology or Metabion. Restriction enzymes and T4 DNA Ligase were obtained from either New England Biolabs or Promega. Total RNA from human tissues was purchased from Clontech or ZenBio (adipose). Cofactors were purchased from Sigma (NAD^+, $NADP^+$, and NADH) and Serva (NADPH). Unlabeled substrates were obtained from Sigma, whereas ^{3}H-labeled substrates were synthesized by American Radiolabeled Chemicals ([1,2-^{3}H]cortisone), Amersham Biosciences (17α-[6,9-^{3}H]estradiol), and PerkinElmer Life Sciences (3α,17β-[9,11-^{3}H]androstanediol, [9,11-^{3}H]androsterone, Δ4-[1,2,6,7-^{3}H]androstenedione, [1,2,6,7-^{3}H]-dehydroepiandrosterone, [1,2,4,5,6,7-^{3}H]dihydrotestosterone; 17β-[6,7-^{3}H]estradiol; [2,4,6,7-^{3}H]estrone; [1,2,6,7-^{3}H]hydrocortisone; [1,2,6,7-^{3}H]progesterone; [1,2,6,7-^{3}H]testosterone). All other chemicals and solvents were purchased from Sigma, Merck, or AppliChem.

Cloning of AKR1B15—The protein-encoding sequences of the *AKR1B15* splice variants *AKR1B15.1* (Ensembl entry *AKR1B15-201*, ENST00000423958) and *AKR1B15.2* (Ensembl entry *AKR1B15-001*, ENST00000457545) were amplified by PCR from cDNA libraries of testis and thymus, respectively, using Phusion High Fidelity polymerase (New England Biolabs) and transcript-specific primers with restriction enzyme sites (Table 1). The PCR products were cloned into pET28a(+) (Novagen) via NdeI/XhoI, into pcDNA3.1(+) (Invitrogen) via NotI/XhoI, into N-Myc-pcDNA3 (modified pcDNA3 with an N-terminal Myc tag) via NotI/XhoI, into pcDNA4-Myc/HisB (Invitrogen) via HindIII/NotI, and into pIRES-hrGFP1α (Stratagene) via NotI/XhoI restriction sites, using HindIII, HindIII-HF, NdeI, NotI-HF, and XhoI restriction enzymes and T4 DNA ligase (New England Biolabs). The complete sequence of the inserts was verified by Sanger sequencing. The sequences obtained were identical to the sequences deposited in the Ensembl database.

Expression and Purification of AKR1B15 Isoforms—His_6-tagged AKR1B15.1 and AKR1B15.2 were expressed in *Escherichia coli* BL21 (DE3), carrying the respective pET28a(+) expression vectors, by induction with 0.5 mM isopropyl 1-thio-β-D-galactopyranoside and overnight incubation at 25 °C. Cell pellets were harvested, resuspended in lysis buffer (50 mM potassium phosphate buffer (KP_i), pH 8.0, 300 mM KCl, 5 mM imidazole, 1% (m/v) *N*-lauroylsarcosine), and lysed by four cycles of 30-s ultrasonication pulses and a 30-s ice bath. The lysate was centrifuged (13,000 × *g*, 4 °C, 30 min), and the resulting supernatant was supplemented with Triton X-100 to a final concentration of 2% and applied on a Profinia affinity chromatography protein purification system (Bio-Rad). The proteins were automatically purified according to the "native IMAC purification protocol for His-tagged proteins" given by the manufacturer with modified buffers (2× wash buffer-1: 100 mM KP_i, pH 8.0, 600 mM KCl, 10 mM imidazole, 0.5% (m/v) *N*-lauroylsarcosine; 2× wash buffer-2: 100 mM KP_i, pH 8.0, 600 mM KCl, 20 mM imidazole, 0.5% (m/v) *N*-lauroylsarcosine; 2× elution buffer: 100 mM KP_i, pH 8.0, 600 mM KCl, 500 mM imidazole, 0.1% (m/v) *N*-lauroylsarcosine; 1× desalting buffer: 20 mM KP_i, pH 7.4, 1 mM EDTA) using a 1-ml Bio-Scale Mini Profinity IMAC cartridge (Bio-Rad) followed by a 10-ml Bio-Scale Mini Bio-Gel P-6 desalting cartridge (Bio-Rad). The final concentration of eluted proteins was determined via the Bio-Rad DC protein assay kit.

Cell Culture and Transfection of Human Cells—HEK293 cells (CRL-1573^{TM}; ATCC) were cultured in DMEM (high glucose, stable glutamine) (PAA), and HeLa cells (ACC57; DSMZ) were cultured in minimum essential medium with Earle's salts (L-glutamine) medium (PAA), both supplemented with 10% FBS Gold (PAA), 100 units/ml penicillin, and 100 μg/ml streptomycin (Invitrogen). BeWo cells (CCL-98^{TM}; ATCC) were cultured in F12-K medium (Invitrogen) supplemented with 10% FBS Gold (PAA). SGBS cells were provided by Prof. M. Wabitsch (36) and cultured in DMEM/F-12 (1:1) (L-glutamine, 15 mM HEPES) medium (Invitrogen) supplemented with 10% FBS Gold (PAA), 17 μM pantothenate, and 33 μM biotin. All cells were maintained at 37 °C, 5% CO_2 in a humidified incubator and trypsinized for continuative cultivation or cell harvest using 0.05% trypsin-EDTA (Invitrogen). Transfections of HEK293 or HeLa cells were carried out using Xtreme DNA 9 transfection reagent (Roche Applied Science) according to the manufacturer's protocols.

Enrichment of Mitochondria from BeWo Cells—Mitochondria were enriched from the BeWo cell line using a pump-controlled cell rupture system, following the protocol published by Schmitt *et al.* (37). For cell rupture, 2×10^7 freshly harvested BeWo cells were resuspended in 4 ml of isolation buffer (300 mM sucrose, 5 mM TES, and 200 μM EGTA, pH 7.2) and passed three times through a cell homogenizer with 10-μm clearance (Isobiotech) at a constant flow of 700 μl/min. Ruptured cells were centrifuged at 800 $\times$ *g* and 4 °C for 5 min. The resulting supernatant was centrifuged once more at 9000 $\times$ *g* and 4 °C for 10 min. The concentration of total protein in the fractions (800 $\times$ *g* pellet, 9000 $\times$ *g* pellet, and 9000 $\times$ *g* supernatant) was determined via the Bio-Rad DC protein assay kit (Bio-Rad).

Generation of Polyclonal and Monoclonal Antibodies against AKR1B15—The peptide sequence corresponding to a region with the most dissimilarity between AKR1B15 and AKR1B10 (Fig. 1*B*, *red box*) was used as antigen for the generation of polyclonal IgG antibodies against AKR1B15 in rabbits, which was carried out by 21st Century Biochemicals (Marlboro, MA). The peptide Ac-NWRAFDFKEFSHLC-amide was synthesized, conjugated to an immune carrier, and used for the immunization of two rabbits to produce polyclonal antisera. Prior to use, the resulting antibodies were affinity-purified via the peptides deployed for immunization.

For the generation of the monoclonal antibody, the peptide comprising the amino acid sequence QGFKTGDDFFPKDDKGNMISGKGTF from the human AKR1B15 protein (Fig. 1*B*, *green box*) was synthesized and coupled to ovalbumin (Peps4LS, Heidelberg, Germany). Lou/c rats were immunized subcutaneously and intraperitoneally with a mixture of 50 μg peptide-ovalbumin, 5 nmol of CPG oligonucleotide (Tib Molbiol, Berlin), 500 μl of PBS, and 500 μl of incomplete Freund's adjuvant. A boost without adjuvant was given 6 weeks after the primary injection. Fusion of the myeloma cell line P3X63Ag8.653 (ATCC; CRL-1580^{TM}) with rat immune spleen cells was performed using standard procedures. Hybridoma supernatants were tested in a differential ELISA with the biotinylated AKR1B15 peptide and an irrelevant biotinylated peptide on avidin-coated ELISA plates. mAbs that reacted specifically with the AKR1B15 peptide were further analyzed by Western blot. Hybridoma culture supernatant of the anti-AKR1B15 clone 9A5 (rat IgG2a subclass) was used in this study.

SDS-PAGE and Western Blotting—Denatured proteins were loaded onto a 12% Mini-Protean or Criterion TGX gel (Bio-Rad) and separated by conventional electrophoresis in running buffer (25 mM Tris, pH 8.3, 192 mM glycine, 0.1% (m/v) SDS). Afterward, gels were either stained via Coomassie Brilliant Blue (0.05% (m/v) Coomassie Brilliant Blue R250, 10% (v/v) acetic acid, 40% (v/v) methanol) or blotted onto a PVDF membrane (Immobilon FL, Millipore) via semidry blot in transfer buffer (48 mM Tris, 39 mM glycine, 0.0375% (m/v) SDS, 20% (v/v) methanol). For testing antibody specificity, membranes after transfer were blocked with 5% skimmed milk powder in PBS and then incubated overnight with primary antibodies in 0.5% skimmed milk powder in PBS at 4 °C. Membranes were washed three times with PBS for 10 min, followed by incubation with HRP-conjugated secondary antibodies (also in 0.5% skimmed milk powder in PBS) and another washing step. Signals were detected by incubating the membranes in Pierce ECL Plus Western blotting substrate (Thermo Scientific) according to the manufacturer's protocol and visualized using a Fusion FX7 system (Vilber Lourmat). A similar procedure was used to detect endogenous AKR1B15 isoforms, except that IR dye-labeled secondary antibodies and an Odyssey infrared imaging system (LI-COR) were used. Briefly, membranes were blocked with 50% Odyssey blocking buffer (for PBS) in PBS after transfer, antibodies were diluted in 50% Odyssey Blocking Buffer (for PBS) in PBS-T (0.05% Tween 20 in PBS), and washing steps were performed with PBS-T.

RNA Isolation and cDNA Synthesis—RNA from cultured cells was isolated using the RNeasy minikit (Qiagen) combined with a DNase I (Qiagen) digestion treatment. 1 μg of RNA was reverse transcribed using oligo$(dT)_{18}$ primers and the AffinityScript qPCR cDNA synthesis kit (Agilent) or avian myeloblastosis virus reverse transcriptase (Promega) according to the manufacturer's protocols.

RT-PCR and qPCR—End point and real-time RT-PCR were carried out both with the same set of transcript-specific primer pairs (Table 1). For the end point RT-PCR, DreamTaq Green DNA polymerase (Thermo) was used according to the manufacturer's protocol, with 38 amplification cycles for *AKR1B* transcripts and 24 cycles for *GAPDH* controls in a RoboCycler (Stratagene). PCR products were analyzed on a 2% agarose gel containing 0.0025% Midori Green (Biozym). qPCR was carried out applying the Perfect CT SYBR Green master mix (Quanta) and a three-step protocol (95 °C for 15 s; 57 °C for 30 s; 72 °C for 45 s) with an ABI 7900 HT instrument. Amplification efficiency was verified for each pair of primers using a standard curve constructed by serial dilution of a control template. Resulting C_T values for *AKR1B15.1*, *AKR1B15.2*, and *AKR1B10* transcripts were corrected by the average C_T value of the three housekeeping genes *GAPDH*, *HPRT*, and *18S RNA* (ΔC_T calculated) and normalized to the expression level of *AKR1B15.1* in placenta.

Activity Assays—Catalytic activity was measured using ^{3}H-labeled steroids either with 10^6 harvested HEK293 cells (untransfected or transfected with pIRES-hrGFP-1α-AKR1B15) or with purified enzymes as described previously (38) with slight mod-

ifications. Reaction assays using HEK293 cells contained 10–40 nM ^{3}H-labeled steroid (PerkinElmer Life Sciences) and generally 350 μM NAD(P)(H) cofactor (Serva, Sigma) in 500 μl of reaction buffer (100 mM sodium phosphate buffer (NaP_i), pH 7.4, 1 mM EDTA). For the determination of Michaelis-Menten parameters, 0–10 μM unlabeled steroid (Sigma) was added. In assay mixtures containing purified proteins (up to 55 nM), 0.05% (m/v) BSA was added. The reaction mixtures were incubated with continuous shaking at 37 °C, and the reaction was terminated by the addition of 20% stop solution (0.5 M ascorbic acid, 1% (v/v) acetic acid in methanol). Steroids were extracted on StrataC18-E (55 μm, 70 Å, 100 mg/ml) SPE cartridges (Phenomenex) with methanol as eluent. Substrates and products were separated by reverse phase HPLC on a Luna 5-μm C18(2) 125 × 4-mm column (Phenomenex) with 43% acetonitrile in MilliQ-H_2O as mobile phase, using a Beckman-Coulter system coupled to an online scintillation detector (Berthold LB506D). Conversion of ^{3}H-labeled substrate was determined from ratios of areas under the peaks by Karat software (Beckman-Coulter).

Activity assays with unlabeled substrates were carried out with purified enzyme by measuring the change in NADPH absorbance at 340 nm using a Cary50 UV-visible spectrophotometer (Varian) as described previously (2). The reaction mixture contained 150 μM NADPH, 6 μM purified enzyme, and substrate at variable concentrations (0–1 mM) in reaction buffer (100 mM NaP_i, pH 7.0, 1 mM EDTA). The reaction was initiated by the addition of substrate to the prewarmed mixture and allowed to run at 37 °C for 10–15 min with continuous absorbance recording. The initial velocity was calculated from the linear portion (0–5 min) of the curve. Kinetic parameters were calculated using SigmaPlot version 12 software (Systat Software).

Fluorescence Titrations—The binding affinity of AKR1B15 isoforms to pyridine nucleotide cofactors was studied fluorometrically by following the quenching of the protein fluorescence (λ_{ex} = 280 nm, λ_{em} = 340 nm) upon the addition of cofactors (39), using a Shimadzu RF5000 instrument. Aliquots containing 14 μg of purified protein (corresponding to a final concentration of 180 or 170 μM for AKR1B15.1 or AKR1B15.2, respectively) were added to 2 ml of 20 mM KP_i, pH 7.4, at room temperature and equilibrated for 15–20 min. Aliquots of nucleotides were added sequentially, and changes in emission were recorded. Dissociation constants were calculated by fitting a Morrison equation (Equation 1) to the data after correction for the volume increase due to the addition of nucleotides and inner filter effect using SigmaPlot version 12 software (Systat software),

$$\Delta F = \Delta F_{max} \cdot \frac{E + N + K_d - \sqrt{(E + N + K_d)^2 - 4 \cdot E \cdot N}}{2 \cdot E} \quad \text{(Eq. 1)}$$

where ΔF represents decrease in protein fluorescence, E is total enzyme concentration, and N is total nucleotide concentration.

Subcellular Localization Studies—HeLa cells were grown on glass coverslips on the bottom of a 6-well plate and transiently transfected with plasmids (pcDNA3.1(+), N-Myc-pcDNA3, or pcDNA4-Myc/HisB backbone) encoding AKR1B15.1 or AKR1B15.2. For counterstaining the cytoplasm and endoplasmic reticulum, pCMV-DsRed-Express2 and pDsRed2-ER (Clontech) vectors were co-transfected, respectively. After transfection, cells were incubated at 37 °C and 5% CO_2 in a humidified incubator for additional 2 days. Mitochondria were counterstained before the cells were prepared for immunocytochemical analysis by incubating living cells in serum-free minimum essential medium with Earle's salts containing Mito-Tracker Orange CMTM-Ros (Molecular Probes) for 30 min. After staining the mitochondria, the cells were fixed in 3.7% formaldehyde in PBS for 10 min at culturing conditions, permeabilized for 5 min using 0.5% Triton X-100 in PBS, and blocked with 3% BSA in PBS for 1 h to prevent nonspecific binding of the antibodies. The fixed cells were consecutively incubated with mouse anti-Myc (Roche Applied Science)/goat anti-rabbit AlexaFluor 488 (Molecular Probes) antibodies in the case of Myc-tagged AKR1B15 isoforms or with rabbit anti-AKR1B15 (21st Century Biochemicals)/goat anti-rabbit AlexaFluor 488 (Molecular Probes) and rat-anti-AKR1B15 clone 9A5 (in-house production)/goat anti-rat AlexaFluor 488 (Molecular Probes) in the case of untagged proteins for 1–2 h. Before mounting objects on slides with VectaShield mounting medium (Vector Laboratories), nuclei were counterstained with Hoechst 33342 dye (Molecular Probes) diluted 1:5000 in PBS for 2 min. After each step, cells were washed twice with PBS. Subcellular localization data were collected and analyzed using a Zeiss AxioImager Z1/ApoTome confocal microscope with an AxioCam MRm camera and the AxioVision release 4.8 software. *In silico* predictions of the localization of AKR1B15 isoforms were carried out using iPSORT for non-plant proteins (40).

RESULTS

Two Splice Variants of AKR1B15 Are Expressed in Vivo—Previously, we reported the identification and functional expression of a novel human member of the AKR1B family with 91% amino acid identity to the well characterized human enzyme AKR1B10 (35). The gene encoding this protein, *AKR1B15*, is located on chromosome 7 next to *AKR1B10.* After our report, a newly predicted transcript sequence corresponding to the *AKR1B15* gene was deposited in the NCBI and Ensembl databases. The predicted transcript is 1621 bp in length and differs from our reported 1242-bp cDNA sequence in the 5′-end. Bioinformatics analysis revealed that the two sequences might result from an alternative use of the first exons of the *AKR1B15* gene, leading to two transcripts, hereafter referred to as *AKR1B15.1* (Ensembl transcript *AKR1B15-201*) for the short and *AKR1B15.2* (Ensembl transcript *AKR1B15-001*) for the long transcript (Fig. 1*A*). To determine whether the alternative transcript *AKR1B15.2*, like *AKR1B15.1*, is expressed *in vivo*, we designed specific primers based on the predicted sequence and amplified the corresponding product by PCR from the cDNA libraries of human thymus and salivary gland. Sequencing of the resulting product confirmed its 100% identity to the sequence reported in the databases. Thus, *AKR1B15.2* mRNA is expressed in tissues and might be translated into a protein because it contains an open reading frame corresponding to a 344-amino acid protein. We conclude that

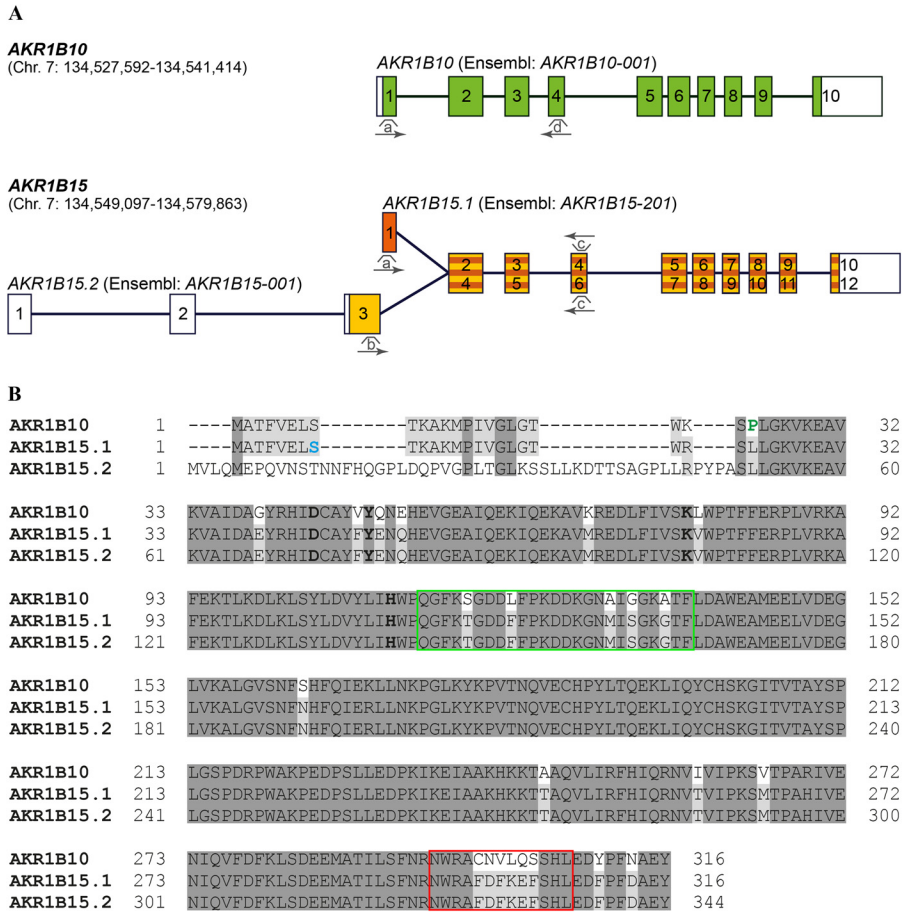

FIGURE 1. **Comparison of *AKR1B10* and *AKR1B15* on gene, transcript, and protein levels.** *A*, schematic illustrations of intron-exon structures of *AKR1B10* and *AKR1B15* genes. Alternative use of exons in the 5′-region of AKR1B15 generates two splice variants, referred to as *AKR1B15.1* (Ensembl transcript *AKR1B15-201*) and *AKR1B15.2* (Ensembl transcript *AKR1B15-001*), which are translated into the protein isoforms AKR1B15.1 and AKR1B15.2, respectively. *Straight black lines* depict introns, whereas exons are shown as *numbered rectangles*. Translated exons of *AKR1B10* are *colored* in *green*, and alternatively spliced exons in the 5′-region of *AKR1B15* are *colored* in *orange* (for *AKR1B15.1*) or *yellow* (for *AKR1B15.2*), followed by *orange-yellow-striped* common exons. UTRs are shown in *white*. *Arrows* depict annealing sites for transcript-specific primer pairs: AKR10–15.1-fwd (*a*), AKR15.2-fwd (*b*), AKR15-rev (*c*), AKR10-rev (*d*). *B*, alignment of the protein sequences of AKR1B10, AKR1B15.1, and AKR1B15.2. Alternative splicing of the 5′-region of AKR1B15 leads to a totally different and longer N terminus of AKR1B15.2 compared with that of AKR1B15.1. AKR1B15.1 and AKR1B10 possess high homology in their N termini. Amino acids of the catalytic tetrad are highlighted in *boldface type*; the serine at position 8 of AKR1B15.1, which is mutated in a phenotype with a mitochondrial disease, is *colored* in *blue*; and the proline at position 24 of AKR1B10, which is responsible for its cytosolic localization, is *colored* in *green*. The recognition region for the monoclonal rat-anti-AKR1B15 antibody is highlighted by a *green box*; the C-terminal recognition region for the polyclonal rabbit anti-AKR1B15 antibody is highlighted by a *red box*.

the *AKR1B15* gene gives rise to two splice variants *in vivo*, presumably coding for two different protein isoforms (Fig. 1), and classify these protein isoforms as AKR1B15.1 (shorter, 316-amino acid isoform, encoded by transcript *AKR1B15.1*) and AKR1B15.2 (longer, 344-amino acid isoform, encoded by transcript *AKR1B15.2*) in accordance with the guidelines for the nomenclature of alternative splicing in the AKR superfamily (41). The two AKR1B15 isoforms differ in their N termini but share the same sequence beginning with the amino acid Ser^{23} in the case of AKR1B15.1 and Ser^{51} in the case of AKR1B15.2 (Fig. 1*B*). The four amino acid residues known to comprise the catalytic tetrad in AKRs are found in both AKR variants (Asp^{44}, Tyr^{49}, Lys^{78}, and His^{111} for AKR1B15.1 and Asp^{72}, Tyr^{77}, Lys^{106}, and His^{139} for AKR1B15.2, respectively; Fig. 1*B*).

Tissue Distribution of AKR1B15—To determine the tissue abundance of the two AKR1B15 isoforms, we first analyzed the expression of the two mRNA splice variants in a broad panel of tissues by RT-PCR, using transcript-specific primers as depicted in Fig. 1*A* (sequences listed in Table 1). For comparison, the expression of the highly homologous *AKR1B10* was analyzed in the same set of samples. We found that the expression of *AKR1B15.1* and *AKR1B15.2* differs completely from that of *AKR1B10*. Whereas *AKR1B10* is expressed in a fairly ubiquitous manner across the tissue panel, the *AKR1B15* variants show more distinct distribution patterns (Fig. 2*A*). The highest expression levels of both *AKR1B15* splice variants were seen in adipose tissue, skeletal muscle, thymus, thyroid gland, and reproductive tissues (ovary, placenta, prostate, and testis). Corroborating the results from tissues, the human placental cell line BeWo and the preadipocyte cell strain SGBS expressed significant levels of both *AKR1B15* transcripts (Fig. 2*A*). In order to gain additional insights into the expression levels of *AKR1B15*, we performed qPCR on selected *AKR1B15*-expressing tissues, using the same transcript-specific primers as for the end point RT-PCR. We found the highest level of expression of both *AKR1B15* mRNA variants in placenta, followed by adipose tissue and testes (Fig. 2*B*). On the absolute level, the abundance of *AKR1B15* mRNA was quite low. In placenta, the tissue with

TABLE 1

Primer names and sequences used for cloning and semiquantitative RT-PCR or qPCR

Restriction sites are underlined, and coding sequences are shown in capital letters. RT, semiquantitative RT-PCR; Q, qPCR.

Primer	Sequence/Description
Primers for cloning into pET28a(+)	
AKR1B15.1-NdeI_fwd	5′-cccttccatATGGCCACGTTTGTGGAGCT-3′
AKR1B15.2-NdeI_fwd	5′-tcaagctacatATGGTCTTACAAATGGAA-3′
AKR1B15-XhoI_rev (1)	5′-agatccctcgagTCAATATTCTGCATCGAA-3′
Primers for cloning into pcDNA3.1(+)	
AKR1B15.1-NotI_fwd (1)	5′-aagaagcggccgcaccATGGCCACGTTTGTGGAGCT-3′
AKR1B15.2-NotI_fwd (1)	5′-aagaagcggccgcaccATGGTCTTACAAATGGA-3′
AKR1B15-XhoI_rev (1)	5′-agatccctcgagTCAATATTCTGCATCGAA-3′
Primers for cloning into N-myc-pcDNA3	
AKR1B15.1-NotI_fwd (2)	5′-ttttgcggccgcaagccacgtttgtggagctc-3′
AKR1B15.2-NotI_fwd (2)	5′-ttttgcggccgcaaGTCTTACAAATGGAACCCCA-3′
AKR1B15-XhoI_rev (2)	5′-tttctcgagTCAATATTCTGCATCGAAGGGAAAGT-3′
Primers for cloning into pcDNA4-myc/HisB	
AKR1B15.1-HindIII_fwd	5′-ttttaagcttatggccacgtttgtggagctc-3′
AKR1B15.2-HindIII_fwd	5′-ttttaagcttATGGTCTTACAAATGGAACCCCA-3′
AKR1B15-NotI_rev	5′-ttttgcggccgctATATTCTGCATCGAAGGGAAAGT-3′
Primers for cloning into pIRES-hrGFP-1α	
pET28-AKR1B15.1-NotI_fwd	5′-aagaagcggccgcaccATGGGCAGCAGCCAT-3′
AKR1B15.2-NotI-His_fwd	5′-aaatggcggccgcaccatgggcagcagccatcatcatcatcatcacagcagcggcctggtgccg gcggcagccatATGGTCTTACAAATGGAACCCCAAGTGAACTCA-3′
AKR1B15-XhoI_rev (1)	5′-agatccctcgagTCAATATTCTGCATCGAA-3′
Primers for RT-PCR and qPCR	
AKR10–15.1_fwd	5′-CCACGTTTGTGGAGCTCAGT-3′ (RT, Q)
AKR15.2_fwd	5′-CCCTTTGACTGGCCTAAAGA-3′ (RT, Q)
AKR10_rev	5′-AACGTTGCTTTTCCACCGATGGC-3′ (RT, Q)
AKR15_rev	5′-AACGTTCCTTTTCCACTGATCAT-3′ (RT, Q)
GAPDH_fwd (1)	5′-agtcaacggatttggtcgta-3′ (RT)
GAPDH_rev (1)	5′-atgacaagcttcccgttct-3′ (RT)
GAPDH_fwd (2)	5′-GGTGGTCTCCTCTGACTTCAACA-3′ (Q)
GAPDH_rev (2)	5′-GTTGCTGTAGCCAAATTCGTTGT-3′ (Q)
HPRT1	RT^2 qPCR primer assay for human HPRT1 (SABiosciences) (Q)
18S RNA	RT^2 qPCR primer assay for human 18 S rRNA (SABiosciences) (Q)

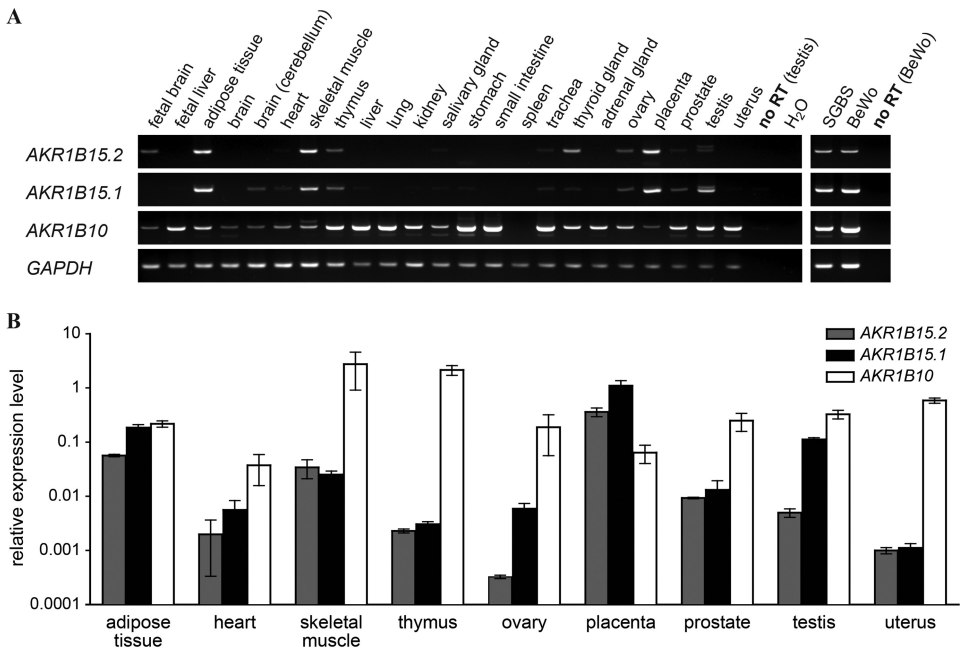

FIGURE 2. **Expression of *AKR1B10*, *AKR1B15.1*, and *AKR1B15.2* in tissues and cell lines.** *A*, semiquantitative end point RT-PCR with cDNA from tissues and cell lines shows different expression patterns for *AKR1B15* and *AKR1B10*. *GAPDH* as well as reactions without reverse transcriptase (*no RT*) or cDNA (H_2O) serve as controls. *B*, quantitative real-time PCR with cDNA of selected tissues validates differences in expression levels of *AKR1B15.1*, *AKR1B15.2*, and *AKR1B10*. Expression levels of *AKR1B15.1* (*black bars*), *AKR1B15.2* (*gray bars*), and *AKR1B10* (*open bars*) transcripts are shown on a logarithmic scale and are normalized to the expression of *AKR1B15.1* in placenta after correction of the C_T values by the average of the three housekeeping genes: *GAPDH*, *HPRT*, and *18S RNA*. *Error bars*, S.D. values from two independent cDNA sets.

the highest level of expression, the abundance of *AKR1B15.1* transcripts was 100–150-fold lower than that of *GAPDH*. In a majority of tissues, the *AKR1B15.1* transcript was more abundant (at least 3-fold) than *AKR1B15.2*. In the thymus, prostate, and uterus comparable levels of both transcripts were found. Skeletal muscle was the only tissue where *AKR1B15.2* showed

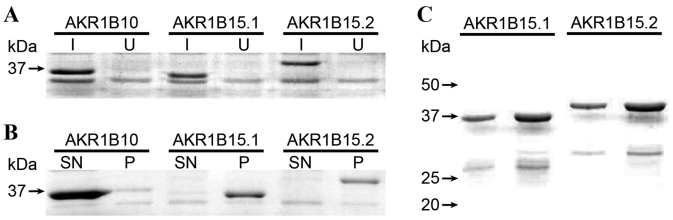

FIGURE 3. **Expression and purification of AKR1B10, AKR1B15.1, and AKR1B15.2 in *E. coli* BL21 (DE3).** Protein bands in Coomassie-stained SDS-polyacrylamide gels are shown. *A*, lysates of isopropyl 1-thio-β-D-galactopyranoside-induced (*I*) but not uninduced (*U*) cell pellets show clear bands of AKR1B10, AKR1B15.1, and AKR1B15.2, respectively. *B*, after centrifugation of induced cell lysates, both AKR1B15 isoforms show up as insoluble proteins in the pellet fraction (*P*), whereas AKR1B10 is soluble and therefore present in the supernatant (*SN*). *C*, purification of AKR1B15.1 and AKR1B15.2 leads to sufficiently pure protein, containing only minute amounts of degradation or truncation products.

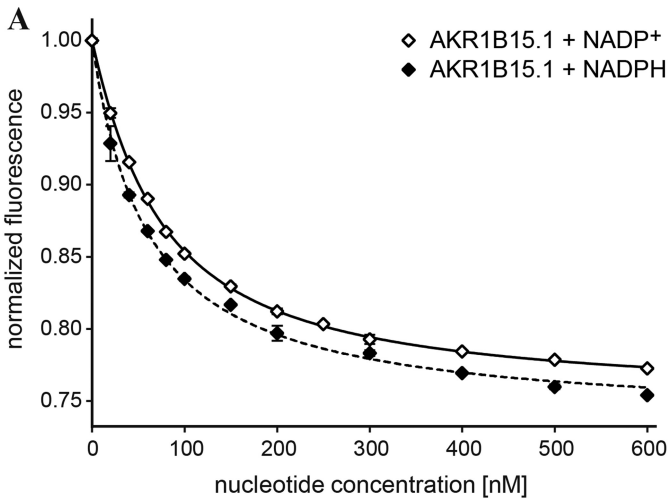

B

	K_d [nM]	max. quenching [%]
NADPH	59 ± 2	26
$NADP^+$	60 ± 4	25
NADH	no binding	< 3
NAD^+	no binding	< 3

FIGURE 4. **Binding of dinucleotide cofactors to AKR1B15.1.** *A*, NADPH (*open diamonds*)- or $NADP^+$ (*filled diamonds*)-dependent decline in the fluorescence of AKR1B15.1 was measured in 20 mM KP_i buffer, pH 7.4, using an excitation wavelength of 280 nm and emission wavelength of 340 nm. Data are shown as discrete points, and curves are best fits of Equation 1 to the data. Changes in fluorescence were normalized to the value of the initial fluorescence of the protein; data are presented as mean ± S.D. (*error bars*) of two independent measurements. B, parameters gained from cofactor titration studies. K_d and maximum quenching (ΔF_{max}) were calculated from the fluorescence curves by fitting Equation 1 to the data.

higher expression than *AKR1B15.1*. Only testis and adipose tissue displayed either of the *AKR1B15* transcripts at a level of more than 10% of that of *AKR1B15.1* in placenta. Skeletal muscle expressed around 2.5% and all other tissues tested had less than 1% of the level found in placenta. Hence, the expression pattern of *AKR1B15* is specific to a few tissues. *AKR1B10* and *AKR1B15*, despite high sequence similarity, display different tissue abundance; among the tissues with *AKR1B15* expression, the abundance of *AKR1B10* mRNA exceeded that of *AKR1B15* by over 500-fold in the lung, thymus, and uterus. In contrast, the expression level of *AKR1B10* was only 6% of that of *AKR1B15.1* in placenta (Fig. 2*B*).

Recombinant Expression and Purification of AKR1B15—To verify that both *AKR1B15* mRNA variants produce functional proteins, we cloned their coding regions into the vector pET28a(+) and expressed encoded His-tagged proteins in *E. coli*. After induction with isopropyl 1-thio-β-D-galactopyranoside, bands with the predicted molecular weights were detected in bacterial extracts transformed with the corresponding constructs (Fig. 3*A*). AKR1B10, which differs only in 27 amino acid residues from AKR1B15.1 (Fig. 1*B*), was also expressed for comparison. In contrast with AKR1B10, which is expressed as soluble protein in *E. coli*, both AKR1B15 isoforms were found in the insoluble fraction (Fig. 3*B*). We were able to solubilize both N-terminally histidine-tagged AKR1B15 isoforms using a Sarkosyl-Triton buffer system and purified both proteins to apparent homogeneity using a one-step immobilized metal (Ni^{2+}) affinity chromatography (Fig. 3*C*). We attributed the minor low molecular weight bands to the degradation or truncation products of AKR1B15 isoforms (Fig. 3*C*). The purification yielded 6–10 mg of protein/liter of bacterial culture.

Nucleotide Binding—To determine the affinities of the two AKR1B15 proteins for nucleotide cofactors, we determined dissociation constants (K_d) of AKR1B15.1 and AKR1B15.2 for the four major pyridine nucleotides NADPH, NADH, $NADP^+$, and NAD^+ using fluorometric titrations. As shown in Fig. 4*A*, the addition of incremental concentrations of NADPH or $NADP^+$ to AKR1B15.1 led to a gradual decrease in protein fluorescence. The maximal degree of fluorescence quenching was 25–26% in both cases, and the K_d values calculated from the concentration dependence of the decrease in fluorescence were 59.3 ± 1.9 nM for NADPH and 60.4 ± 3.5 nM for $NADP^+$. In contrast, less than 3% quenching of AKR1B15.1 fluorescence was observed with NADH and NAD^+ in concentrations of up to 40 μM after correction for inner filter effect (Fig. 4*B*; titration curve not shown). These results indicate that, like other AKRs, AKR1B15.1 binds pyridine dinucleotides with high affinity and that it strongly discriminates between phosphorylated and non-phosphorylated nucleotides. The addition of any of the four nucleotides to AKR1B15.2 failed to produce any change in protein fluorescence, in agreement with the lack of detectable enzymatic activity of AKR1B15.2 (see below).

Enzymatic Activity of AKR1B15 Isoforms—We performed detailed kinetic characterizations of both AKR1B15 isoforms, AKR1B15.1 and AKR1B15.2, using a variety of physiological substrates.

Because AKR1B15 is abundant in reproductive organs (the first full-length AKR1B15 transcript was initially found in testis), we reasoned that the protein might possess enzymatic activity with sex steroids. Therefore, we tested estrogens, androgens, progesterone, and corticosteroids as potential substrates of AKR1B15.1 or AKR1B15.2. In activity assays using HEK293 cells, transiently transfected with pIRES-hrGFP1α-AKR1B15.1 or pIRES-hrGFP1α-AKR1B15.2 and NADP(H) or NAD(H) as cofactor, we found that neither AKR1B15.1 nor AKR1B15.2 was able to reduce or oxidize progesterone and corticosteroids (data not shown). However, AKR1B15.1 cata-

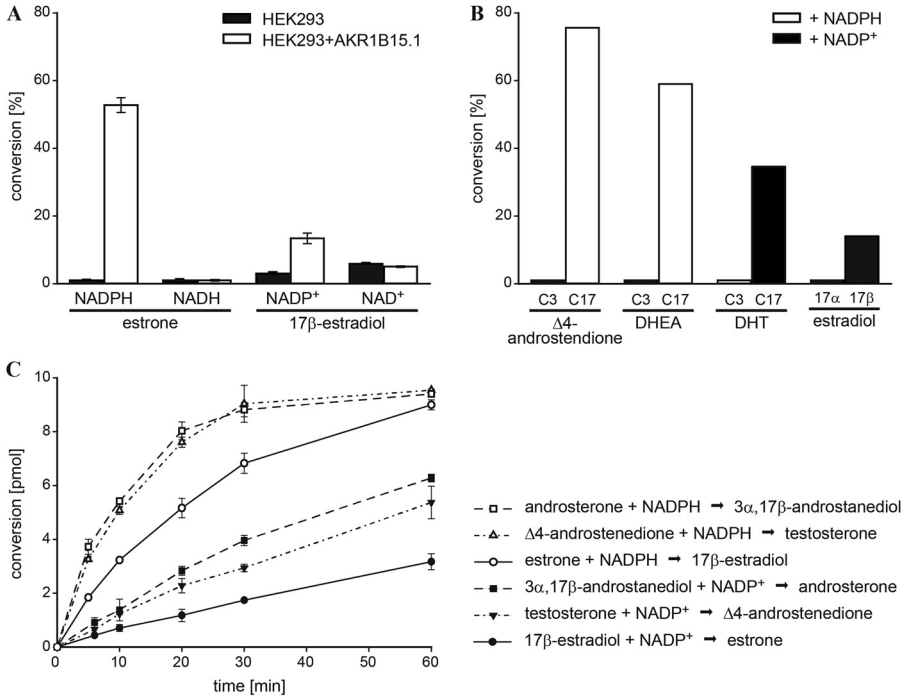

FIGURE 5. **AKR1B15.1 catalyzes redox reactions with steroids.** *A*, AKR1B15.1 exhibits a strong preference for phosphorylated cofactor by catalyzing redox reactions only in the presence of NADP(H) but not NAD(H). Activity tests were carried out using 10^6 HEK293 cells either non-transfected (HEK293) or transiently transfected with pIRES-hrGFP-1α-AKR1B15.1 (HEK293 + AKR1B15.1), 15 nM ^{3}H-labeled estrone or 10 nM ^{3}H-labeled 17β-estradiol, and 350 μM cofactor in reaction buffer. *Bars*, mean of steroid conversion in percentage after 60-min (for estrone) and 120-min (for 17β-estradiol) incubation; *error bars*, S.D. of three replicates. *B*, AKR1B15.1 possesses activity on the C17 β-position of the steroid nucleus (*C17*) but not on the C3 position (*C3*). Activity tests were carried out using 10^6 HEK293 cells transiently transfected with pIRES-hrGFP-1α-AKR1B15.1, 10–40 nM ^{3}H-labeled steroids, and 350 μM NADPH (+ *NADPH*) or $NADP^+$ (+ *$NADP^+$*) cofactor in reaction buffer. *Bars*, conversion in percentage. *C*, comparison of reaction velocities with different steroids. Activity tests were carried out using 90 nM purified AKR1B15.1, 20 nM (corresponding to 10 pmol/reaction) ^{3}H-labeled steroids, and 300–325 μM cofactors in reaction buffer. Results of reductive reactions using NADPH are represented by *open symbols*, and those of oxidative reactions using $NADP^+$ are shown by *filled symbols*. Data represent mean ± S.D. ($n = 3$). *DHEA*, dehydroepiandrosterone; *DHT*, dihydrotestosterone.

lyzed oxidation-reduction reactions with androgens and estrogens, as shown for the estrone and 17β-estradiol pair (Fig. 5*A*). Catalysis was supported by NADPH or $NADP^+$ but not by NADH or NAD^+ (up to a concentration of 1.5 mM), which agrees with the binding studies, suggesting that, similar to a majority of other AKRs, AKR1B15 exhibits a strong preference for phosphorylated cofactors. In addition, we found that AKR1B15.1 possesses high positional selectivity because it catalyzed only reactions on the C17(β) position (*C17*) but not on the C3 position (*C3*) of the steroid nucleus (Fig. 5*B*). In time course experiments using purified AKR1B15.1 and estrogens as well as androgens in a final concentration of 20 nM, we found that AKR1B15.1 prefers reductive over oxidative reactions and androgens over estrogens (Fig. 5*C*). In contrast to AKR1B15.1, AKR1B15.2 did not exhibit any enzymatic activity with estrogens, androgens, or other steroids tested. Because neither the activity assays using solubilized purified AKR1B15.2 nor the assays using HEK293 cells, in which AKR1B15.2 was expressed under physiological conditions, showed any enzymatic activity, it appears that the protein is catalytically inactive, and the lack of activity of the protein purified from bacteria could not be attributed to improper folding.

Because we found that AKR1B15.1 co-localizes with mitochondria (see below), we tested whether the enzyme displays catalytic activity with mitochondrial carbonyls or alcohols, such as acetoacetyl-CoA, oxaloacetic acid, 2-oxobutyric acid, methylmalonyl-CoA, succinyl-CoA, DL-3-hydroxybutyryl-CoA, and DL-3-hydroxy-3-methylglutaryl-CoA. We found that AKR1B15.1, but not AKR1B15.2, possessed enzymatic activity with acetoacetyl-CoA, whereas all other compounds were not detectably reduced or oxidized by either isoform (data not shown). These results indicate that AKR1B15.1 acts only on hydroxyl or keto groups of substrates possessing a bulky ring system like the steroid nucleus or the CoA.

We also determined kinetic parameters of AKR1B15.1 with different substrate classes using the purified enzyme (Table 2). The K_m values for oxidized steroids carrying a keto group on

TABLE 2

Kinetic parameters of AKR1B15.1

Kinetic parameters of AKR1B15.1 were determined with purified enzyme and cofactor NADPH (300 μM) for reductive reactions or $NADP^+$ (325 μM) for oxidative reactions. K_m and k_{cat} values were calculated by Michaelis-Menten fit (SigmaPlot) of initial reaction velocities measured with increasing concentrations of either unlabeled steroids, added to 10 pmol of ^{3}H-labeled steroids, or unlabeled acetoacetyl-CoA. K_m, Michaelis constant; k_{cat}, turnover number; k_{cat}/K_m, catalytic efficiency. Values are mean ± S.E. ($n = 3$).

Substrate	K_m	k_{cat}	k_{cat}/K_m
	μM	min^{-1}	$\mu M^{-1}\ min^{-1}$
Reductive reactions			
Androsterone	2.8 ± 0.2	1.7 ± 0.1	0.61
Δ4-Androstenedione	1.9 ± 0.2	1.1 ± 0.1	0.60
Estrone	2.5 ± 0.4	1.0 ± 0.1	0.38
Acetoacetyl-CoA	63.4 ± 7.4	0.5 ± 0.1	0.01
Oxidative reactions			
3α,17β-Androstandiol	19.2 ± 2.3	3.0 ± 0.3	0.16
Testosterone	7.1 ± 1.5	0.6 ± 0.1	0.09
17β-Estradiol	9.1 ± 1.2	0.5 ± 0.1	0.06

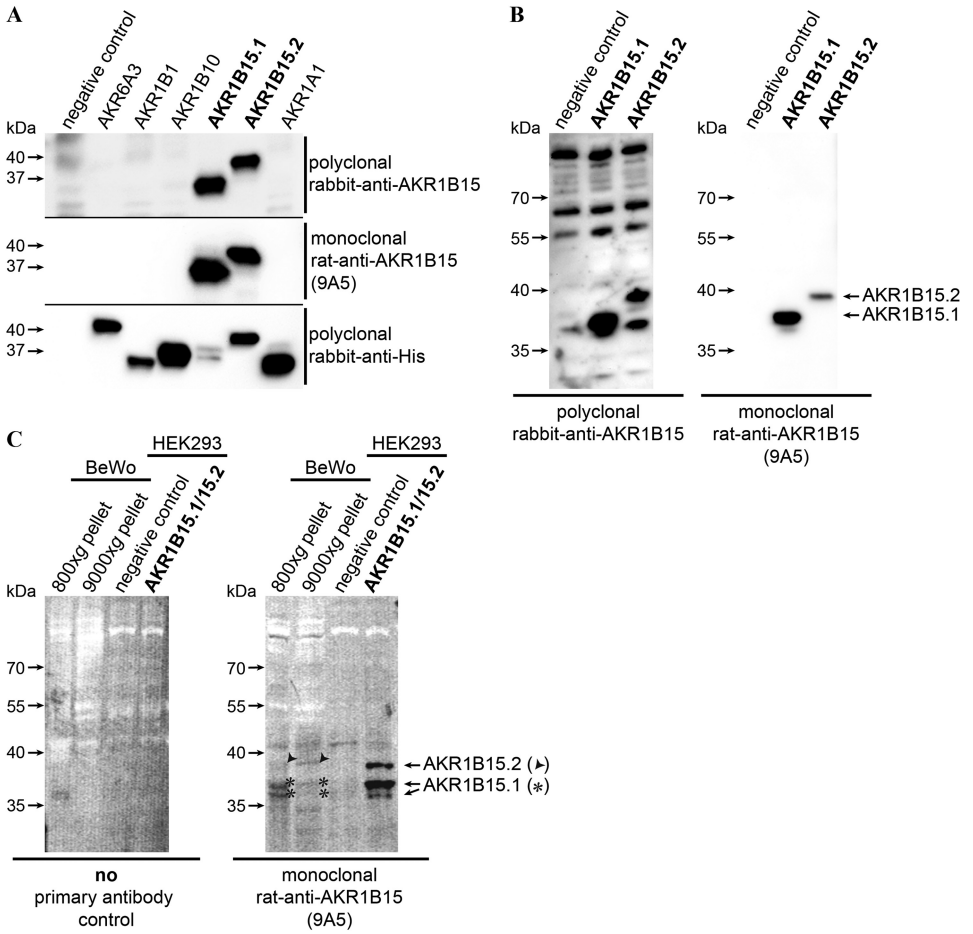

FIGURE 6. **Generation of specific polyclonal and monoclonal anti-AKR1B15 antibodies and detection of endogenous AKR1B15 isoforms.** *A*, different His-tagged human AKRs (AKR6A3, AKR1B1, AKR1B10, AKR1B15.1, AKR1B15.2, and AKR1A1) were expressed in *E. coli* BL21 (DE3) and analyzed by Western blot using polyclonal rabbit anti-AKR1B15, monoclonal rat anti-AKR1B15 (9A5), or polyclonal rabbit anti-His tag (Cell Signaling) antibodies as primary antibodies and HRP-conjugated goat anti-rabbit (Invitrogen) and mouse anti-rat IgG2A (in-house production) secondary antibodies. Non-transformed *E. coli* BL21 (DE3) served as negative control. The anti-His tag staining showed that all proteins were expressed (*bottom*). *B*, untagged AKR1B15.1 and AKR1B15.2 were overexpressed in HEK293 cells and analyzed by Western blot using polyclonal rabbit anti-AKR1B15 and monoclonal rat anti-AKR1B15 (9A5) antibodies as primary antibodies and goat anti-rabbit (Invitrogen) and mouse anti-rat IgG2A (in-house production) antibodies as HRP-conjugated secondary antibodies, respectively. Non-transfected HEK293 cells served as negative control. Whereas the polyclonal antibody is fairly nonspecific, because it recognizes several proteins, the monoclonal antibody shows high specificity to both AKR1B15 isoforms with no cross-reactivity. *C*, fractions (800 × *g* and 9000 × *g* pellets) of the enrichment of mitochondria from BeWo cells were analyzed for the presence of endogenous AKR1B15 isoforms by Western blot using monoclonal rat anti-AKR1B15 (9A5) antibody as primary and IR dye-conjugated goat anti-rat AlexaFluor 790 (Dianova) antibody as secondary (*right panel*). A mixture of extracts from HEK293 cells overexpressing untagged AKR1B15.1 or AKR1B15.2 served as a positive control, and non-transfected HEK293 cells as well as a secondary antibody-only hybridization (*left panel*) served as negative controls. *Asterisk*, endogenous AKR1B15.1; *arrowhead*, endogenous AKR1B15.2.

C17 appeared to be in the low micromolar range (1.9–2.8 μM), whereas reduced steroids carrying a hydroxyl group on C17 showed a 4–7-fold higher K_m (7.1–19.2 μM). The turnover numbers (k_{cat} values) mirrored the results of the time course experiments; k_{cat} values of androgens (0.6–3.0 min^{-1}) were higher than those of estrogens (0.5–1.0 min^{-1}), and, with the exception of the k_{cat} of 3α,17β-androstandiol, k_{cat} values of reductive reactions were about 2-fold higher than those of oxidative reactions. Estimates of the catalytic efficiencies (k_{cat}/K_m) support the conclusion that the protein has higher reductase than dehydrogenase activity. With acetoacetyl-CoA, the enzyme had a K_m value of 63.4 μM and a k_{cat} of 0.5 min^{-1}. The catalytic activity in the reverse direction, oxidation of 3-hydroxybutyryl-CoA, was below our detection limit (0.1 min^{-1}). AKR1B15.2 showed no activity with any of the substrates tested.

Generation of AKR1B15-specific Antibodies and Western Blot Analysis—To examine the expression and the subcellular localization of AKR1B15 proteins, we first generated a specific polyclonal antibody that recognizes both AKR1B15 isoforms and distinguishes them from other AKR family members. Although the amino acid sequence of AKR1B15.1 is 91% identical to that of AKR1B10, there is a single stretch of six consecutive amino acids at the C terminus of the proteins (amino acids 299–304) that is different between the two proteins. Using a peptide corresponding to this area (AKR1B15.1, amino acids 295–307; AKR1B15.2, amino acids 323–335; Fig. 1*B*), we were able to generate a polyclonal antibody that recognized both AKR1B15.1 and AKR1B15.2 but did not cross-react with other recombinant human AKR proteins (Fig. 6*A*). This polyclonal antibody did not cross-react with AKR1B10 even when loading high amounts (200 ng) of purified protein (data not shown). In West-

ern blot analysis of HEK293 transiently transfected with different plasmids encoding either AKR1B15.1 or AKR1B15.2, we could clearly detect the different overexpressed AKR1B15 isoforms. However, the polyclonal antibody also bound nonspecifically to other proteins of the HEK293 cells, including those having a molecular weight similar to that of the AKR1B15 isoforms (Fig. 6*B*, *left*). Because the high cross-reactivity of the polyclonal antibody could complicate the analysis of the expression of the native AKR1B15 proteins and because we found that antibodies against C-terminal sequences often cross-react with several other proteins, we generated a monoclonal antibody (rat anti-AKR1B15 (9A5)) recognizing both AKR1B15 isoforms and targeting a sequence more centrally located in the protein (AKR1B15.1, amino acids 114–138; AKR1B15.2, amino acids 142–166) with high divergence compared with AKR1B10 (Fig. 1*B*). Like the polyclonal antibody, the monoclonal antibody also recognized both AKR1B15.1 and AKR1B15.2 and did not cross-react with other recombinant human AKRs (Fig. 6*A*). In contrast with the polyclonal antibody, the monoclonal antibody displayed no cross-reactivity with proteins of the HEK293 cell background when Western blots were performed (Fig. 6*B*, *right*). To examine whether the mRNA of *AKR1B15* is translated to a protein *in vivo*, we performed Western blots of BeWo cell extracts using the specific monoclonal antibody and an IR dye-labeled secondary antibody (goat anti-rat AlexaFluor 790), which allows for the sensitive detection of low abundance proteins. Although no endogenous AKR1B15 isoforms were detectable in total cell lysates (data not shown), we were able to detect endogenous AKR1B15.1 and AKR1B15.2 in both the 800 × *g* and the 9000 × *g* pellet fraction of BeWo homogenates processed for the enrichment of mitochondria (Fig. 6*C*). Whereas AKR1B15.2 appeared as a single protein band at the expected molecular mass of 39.5 kDa, endogenous as well as overexpressed AKR1B15.1 was present as a double band corresponding to molecular masses of 36.5 kDa (expected) and 35.5–36 kDa, which could be a proteolyzed or post-translationally modified form of the protein.

Subcellular Localization of AKR1B15 Isoforms—To characterize the two AKR1B15 isoforms in more detail, we determined their subcellular localization in the HeLa cell line overexpressing AKR1B15 isoforms using different constructs by immunocytochemistry. We found N- and C-terminally tagged AKR1B15.2 (expressed from N-Myc-pcDNA3-AKR1B15.2 and pcDNA4-Myc/HisB-AKR1B15.2, respectively) in the cytosol (Fig. 7, *a* and *c panels*). A cytosolic localization was observed also for AKR1B15.1 but only when fused to an N-terminal Myc tag (expressed from N-Myc-pcDNA3-AKR1B15.1; Fig. 7, *b panels*). C-terminally tagged AKR1B15.1 (expressed from pcDNA4-Myc/HisB-AKR1B15.1) co-localized with mitochondria (Fig. 7, *d panels*), indicating that the N-terminal amino acid sequence, which is different from that of AKR1B15.2, is important for the mitochondrial localization of AKR1B15.1. These results are in accord with theoretical analysis of AKR1B15 localization using the iPSORT prediction algorithm. The algorithm predicted a mitochondrial localization of AKR1B15.1 and a cytosolic localization of AKR1B15.2 when considering the N-terminal amino acid leader sequences Met^{1}–Glu^{30} and Met^{1}–Leu^{30}, respectively. The mitochondrial localization of AKR1B15.1 (Fig. 7, *f* and *h panels*) and cytosolic localization of AKR1B15.2 (Fig. 7, *e* and *g panels*) was verified in HeLa cells transiently transfected with untagged AKR1B15.1 (pcDNA3.1(+)-AKR1B15.1) or AKR1B15.2 (pcDNA3.1(+)-AKR1B15.2) and stained with either the polyclonal rabbit anti-AKR1B15 antibody or the monoclonal rat anti-AKR1B15 antibody. Thus, AKR1B15.1 is the first AKR localized to the mitochondria.

DISCUSSION

In this work, we demonstrate that a novel human gene, *AKR1B15*, a member of the AKR superfamily, is expressed in human tissues, with the highest level found in reproductive organs, adipose tissue, and skeletal muscle. In addition, we found that the *AKR1B15* gene undergoes alternative splicing, producing two open reading frames corresponding to the protein isoforms AKR1B15.1 and AKR1B15.2. Both mRNA transcripts are expressed *in vivo*, although expression of both variants is limited in abundance and is not as ubiquitous as that of the highly homologous *AKR1B10*. For the most part, the transcript *AKR1B15-201* (referred to as *AKR1B15.1*, encoding protein AKR1B15.1) was more abundant than *AKR1B15-001* (referred to as *AKR1B15.2*, encoding protein AKR1B15.2) in tissues expressing both variants.

Using the monoclonal rat anti-AKR1B15 (9A5) antibody, generated in house, we were able to show that both *AKR1B15* transcripts are translated into protein *in vivo*. Consistent with the low expression of mRNA, the abundance of the AKR1B15 protein was low as well; therefore, fractionation of subcellular components was necessary to detect the endogenous protein. Nevertheless, we were able to identify both endogenous AKR1B15 protein isoforms in the 800 × *g* and 9000 × *g* pellet of homogenates of the placenta-derived BeWo cells but were unable to detect endogenous AKR1B15 isoforms in commercial total protein human tissue lysates and total lysates of BeWo cells (data not shown). It appears that additional steps, such as enrichment of subcellular components or immunoprecipitation, will be necessary to characterize the expression of AKR1B15 in tissues and overcome its low abundance. Additionally, the detection of the proteins could be confounded by post-translational modifications, which could reduce the affinity of the monoclonal antibody to the endogenous protein. Post-translational prediction algorithms indicated that both AKR1B15 isoforms could undergo various modifications (*e.g.* phosphorylation, SUMOylation, or ubiquitination) at several sites, including residues of the monoclonal antibody epitope (data not shown). These modifications could shift the apparent molecular weight of the proteins, destabilize the proteins, or prevent antibody binding and thus interfere with the detection of endogenous AKR1B15 proteins. Additional research is required to investigate these possibilities.

Importantly, AKR1B15.1 showed enzymatic activity with sex steroids, both androgens and estrogens, and 3-keto-acyl-CoA thioesters, such as acetoacetyl-CoA. In contrast, AKR1B15.2 appeared to be an inactive enzyme, despite the fact that it possesses all four conserved amino acid residues of the catalytic tetrad (Asp^{72}, Tyr^{77}, Lys^{106}, and His^{139}). These findings are corroborated by the inability of AKR1B15.2 to bind nicotinamide

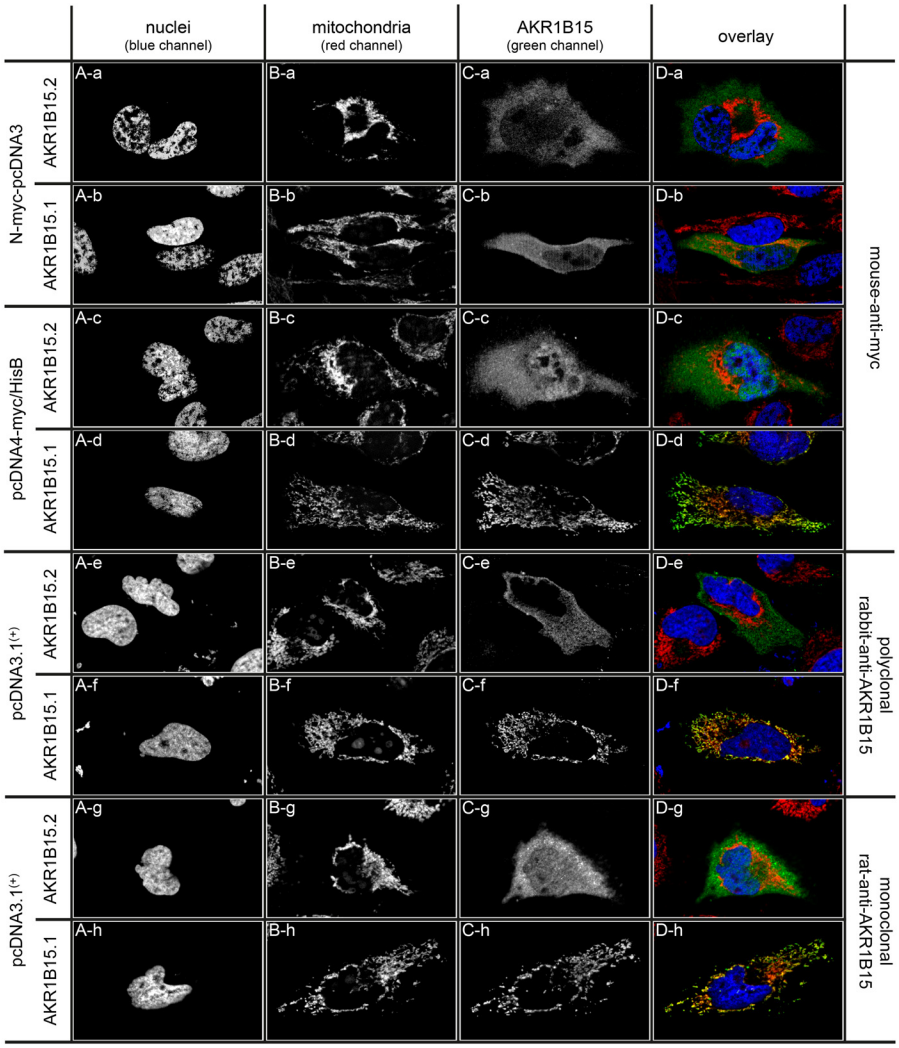

FIGURE 7. **Subcellular distribution of the two AKR1B15 isoforms.** HeLa cells were transiently transfected with either N-Myc-pcDNA3-AKR1B15.2 (*a*), N-Myc-pcDNA3-AKR1B15.1 (*b*), pcDNA4-Myc/His B-AKR1B15.2 (*c*), pcDNA4-Myc/His B-AKR1B15.1 (*d*), pcDNA3.1(+)-AKR1B15.2 (*e* and *g*), or pcDNA3.1(+)-AKR1B15.1 (*f* and *h*) in order to overexpress N-terminally Myc-tagged (*a* and *b*), C-terminally Myc-tagged (*c* and *d*), or untagged (*e*–*h*) protein. *A*, nuclei were stained using Hoechst 33342 dye; *B*, mitochondria were stained using Mito-Tracker Orange CMTM-Ros; *C*, Myc-tagged AKR1B15.1 or AKR1B15.2 was stained using mouse anti-Myc/goat anti-mouse-AlexaFluor 488 antibodies and untagged AKR1B15.1 was stained using polyclonal rabbit anti-AKR1B15/goat anti-rabbit AlexaFluor 488 antibodies or monoclonal rat anti-AKR1B15/goat anti-rat AlexaFluor 488 antibodies. The individual staining as well as the overlays (*D*) demonstrate that AKR1B15.2 is a cytoplasmic protein, whereas C-terminally Myc-tagged AKR1B15.1 as well as untagged AKR1B15.1 co-localize with mitochondria. Nuclei are shown in *blue*, mitochondria in *red*, AKR1B15 in *green*, and co-localization in *yellow*.

adenine dinucleotide cofactors, whereas AKR1B15.1 binds NADPH and $NADP^+$ with an affinity in the nanomolar range. AKR1B15.1 displayed absolute specificity for phosphorylated dinucleotide cofactors because neither binding nor activity has been observed with NADH or NAD^+.

Currently, it is difficult to distinguish whether the lack of nucleotide binding by AKR1B15.2 is due to improper folding or to an intrinsic property of this protein. The undetectable enzymatic activity in both the artificial bacterial and the mammalian expression system supports the latter hypothesis, suggesting that the long N terminus influences the protein structure in such a way that it prevents nucleotide and/or substrate access or binding. Whereas the shorter AKR1B15 isoform, AKR1B15.1, like all other known AKR1B family members, is 316 amino acids long and shares 91% amino acid sequence identity with AKR1B10, the AKR1B15.2 isoform displays greater differences because the N terminus of AKR1B15.2 has no homology with other AKR1Bs and is 28 residues longer. In the crystal structure of AKR1B proteins, the N terminus folds into a hairpin of two β-sheets and creates a bottom of the $(\beta/\alpha)_8$ barrel (2, 42, 43). The alternative N terminus in AKR1B15.2 substitutes the first 22 amino acid residues of other AKR1Bs, which might lead to a disarrangement of the bottom hairpin and the first β-sheet of the $(\beta/\alpha)_8$ barrel. This suggests the intriguing possibility that the N terminus of AKR1B15.2 might serve as a modulatory domain, regulating access to the active site, by changing its conformation in response to protein modification, such as phosphorylation. Alternatively, the non-homologous N-terminal loop of AKR1B15.2 may perform some additional function, analogous to the N terminus of AKR6 family members (Kvβ proteins), which forms a "ball and chain" structure involved in the regulation of ion flow kinetics of voltage-gated potassium (Kv) channels (44, 45). Further investigation is needed to systematically address these possibilities.

Our measurements of enzymatic parameters show that AKR1B15.1 possesses K_m values in the low micromolar range for 17-keto-steroids, which are similar to the K_m values of other 17β-hydroxysteroid dehydrogenases (17β-HSDs) (*e.g.* HSD17B1, HSD17B5, and HSD17B12) (46–48). We found that the enzyme is selective toward the carbonyl group located at the C17 position on the steroid nucleus. The comparatively low k_{cat} values observed with purified enzyme may result from the purification procedure because AKR1B15.1 expressed in *E. coli* is an insoluble protein that needs to be reconstituted from inclusion bodies. In our k_{cat} calculations, we assumed that all protein molecules are properly folded; however, it is more likely that only a fraction of the purified enzyme is in the right conformation. Due to the high homology between AKR1B15.1 and AKR1B10 and the fact that estrogens and androgens are substrates of AKR1B15.1, we measured the activity of purified AKR1B10 with estrone, 17β-estradiol, Δ4-androstenedione, and testosterone. Although it has been published that AKR1B10 is inhibited by steroids (49), we found that AKR1B10 is able to catalyze oxidation or reduction of those steroids in the nanomolar range too. However, in contrast to AKR1B15, AKR1B10 preferentially catalyzed oxidative reactions of steroids (data not shown).

Our studies revealed that AKR1B15.1 is a predominantly reductive enzyme and that it co-localizes with mitochondria. The subcellular localization was surprising because most other human AKRs are cytosolic enzymes. Although *in silico* subcellular localization prediction is hypothetical and often does not agree with *in vivo* localization (50), iPSORT predicted a mitochondrial localization of AKR1B15.1 as well as a cytosolic localization of AKR1B15.2 and AKR1B10, which is in agreement with our results. The different behavior of AKR1B15.1 and AKR1B10 concerning localization can probably be explained by the different amino acid composition in their N termini at positions 22 and 24. AKR1B15.1 possesses an arginine at position 22, and AKR1B10 features a lysine at this position, both of which have similar physicochemical properties. In contrast, the physicochemical properties of the amino acids at position 24 of AKR1B15.1 (Leu^{24}) and AKR1B10 (Pro^{24}) are clearly different. Several previous studies have shown that proline residues serve as a helix breaker (51, 52). We therefore presume that Pro^{24} may be the amino acid responsible for different localization of AKR1B15.1 and AKR1B10. *In silico* prediction with iPSORT indicated a mitochondrial location of the AKR1B10 P24L mutant. This was confirmed in localization studies with N-terminal sequences fused to GFP, in which we were able to show that the substitution P24L in the N terminus of AKR1B10 was sufficient to switch the subcellular localization of the respective GFP reporter construct from cytosolic to mitochondrial (data not shown). The results of Western blotting were consistent with the mitochondrial localization of AKR1B15.1 because endogenous AKR1B15.1 was detected in the 800 $\times$ *g* and 9000 $\times$ *g* pellets of BeWo cell homogenates. The 800 $\times$ *g* pellet contains the nuclear fraction together with unbroken cells, cell debris, and remains of the supernatant, whereas the 9000 $\times$ *g* pellet represents the mitochondrial fraction (37). Surprisingly, AKR1B15.2, which seems to be localized to the cytosol by immunohistochemistry, was found mainly in the 9000 $\times$ *g* pellet rather than the supernatant, suggesting strong association with subcellular organelles, possibly lysosomes, which are likely to be found in the 9000 $\times$ *g* pellet (37).

Among the AKRs, only AKR7A2 has been suggested to be associated with mitochondria in SH-SY5Y neuroblastoma cells (53). However, its rat ortholog, AKR7A4, has also been reported to be localized to the Golgi apparatus (54); therefore, the subcellular localization of this enzyme is still unclear. Hence, we conclude that we characterized the first AKR1 family member co-localizing with mitochondria; however, it still needs to be clarified whether AKR1B15.1 is located inside the mitochondria or strongly associated with the outer membrane.

Having established that AKR1B15.1 is localized to the mitochondria, we investigated whether mitochondria-specific carbonyls are potential substrates of the enzyme. We found that a 3-keto-acyl-CoA compound, acetoacetyl-CoA, can be reduced by AKR1B15.1 with a K_m of about 60 μM. We presume that AKR1B15.1 possesses low oxidizing activity with DL-3-hydroxybutyryl-CoA too, although the conversion could not be detected by our assays, probably due to limitations in the sensitivity of the readout of our assay, which is based on NADPH absorption. Longer chain 3-keto-acyl-CoAs, such as 3-keto-palmitoyl-CoA, could also serve as substrates of AKR1B15.1. However, up to now we were unable to verify the proposed conversion due to limitations in substrate amounts and lack of sensitive and stable detection assays. Development of a more sensitive assay, possibly based on product detection rather than nucleotide absorbance, is necessary to confirm the reaction. The free oxo-(di)-carboxylic acids oxaloacetic acid and 2-oxobutyric acid as well as the CoA-thioesters of dicarboxylic acids methylmalonyl-CoA and succinyl-CoA do not appear to be substrates of AKR1B15.1. This indicates that only carbonyl and not carboxyl groups can be reduced by AKR1B15.1. Moreover, it seems likely that all substrates need to possess a bulky ring backbone for their orientation in the substrate binding pocket of AKR1B15.1.

Although it might seem surprising that a single enzyme reduces such unrelated compounds as steroids and keto-acyl-CoA derivatives, it appears that many 17β-HSDs exhibit a wide substrate spectrum, which includes fatty acid derivatives, bile acids, and retinoids (55). The 17β-HSDs belong to two genetic superfamilies: AKRs and short-chain dehydrogenases (56). To date, at least 14 types of 17β-HSDs have been identified, among which only type 5 belongs to the AKR superfamily (AKR1Cs). No activity with 3-keto-acyl-CoAs has been reported for AKR1C enzymes; however, 17β-HSDs of types 3, 4, 10, and 12, which belong to the short-chain dehydrogenase superfamily, possess activity with both steroids and keto-acyl-CoA conjugates (55). Therefore, we propose that although structurally a member of the AKR superfamily, AKR1B15.1 functionally is a 17β-hydroxysteroid dehydrogenase. Among the human 17β-HSDs, HSD17B10 is a mitochondrial enzyme and catalyzes the NAD-dependent oxidoreduction of short-chain 3-keto-acyl-CoAs, along with sex steroids, as well as bile acid isomerization and glucocorticoid and gestagen catabolism (57). This enzyme is also called SCHAD (short-chain hydroxyl-acyl-CoA dehydrogenase), and it acts primarily in oxidative direction. Defects in this enzyme lead to hyperinsulinemic hypoglycemia (58, 59), abnormal thermogenesis, and lower body weight in mice (60) as

well as neural disorders such as Alzheimer and Parkinson diseases, mental retardation, and infantile neurodegeneration (61).

It could be argued that the results from the activity tests are somehow inconsistent with the subcellular localization of AKR1B15.1 because AKR1B15.1 preferably catalyzes reductive reactions, but the mitochondrial matrix has an oxidative environment, where among other reactions, β-oxidation of fatty acids and the very first steps of the steroid synthesis (from cholesterol to pregnenolone) take place (62). However, with the current data, the role of AKR1B15.1 in mitochondria can only be hypothesized. Different studies have shown that steroids and steroid receptors are present in mitochondria and affect their metabolism (63–65). One function of AKR1B15.1 may be the activation of the steroid signaling in mitochondria, as AKR1B15.1 catalyzes, among other reactions, the conversion of biologically low active estrone to highly active 17β-estradiol, which binds to the mitochondrial estrogen receptor with high affinity (65). Like the nuclear genome, the mitochondrial genome contains hormone-responsive elements (*e.g.* the estrogen response element), regulating the expression of important ribosomal and structural proteins, as well as mitochondrially encoded proteins of the oxidative phosphorylation system (64, 66, 67). In addition, several studies have shown that 17β-estradiol protects the function of mitochondria in cells by reducing the amount of reactive oxygen species and therefore prevents cells from aging (64). Thus, AKR1B15.1 might provide the active steroid hormones that are known to reduce aging in mitochondria and cells. This hypothesis is supported by a recent publication by Yashin *et al.* (68), correlating an SNP in *AKR1B15* with longevity. Another function of AKR1B15.1 might relate to the reduction of 3-keto-acyl-CoAs, such as acetoacetyl-CoA. Reduction of 3-keto-acyl-CoAs is an important step in fatty acid synthesis although not expected in mitochondria, where the reverse process, the β-oxidation of fatty acids, takes place. However, several investigators have been able to show that *de novo* fatty acid synthesis does occur in mitochondria via the FAS II pathway (69–71) and that components of the FAS II pathway might interact with Complex I of the respiratory chain (72).

It has been recently reported that a naturally occurring mutation in the *AKR1B15* gene (leading to an S8R mutation in AKR1B15.1; Fig. 1*B*) is linked to an infantile mitochondrial disease characterized by severe depletion of Complex I activity (73). Interactions between AKR1B15.1 and Complex I would explain why the mutation was associated with this infantile lethal phenotype (73). Here, direct protein-protein interactions in addition to the enzymatic activity of AKR1B15.1 might be of importance.

In conclusion, AKR1B15 is a novel member of the AKR superfamily with potential roles in steroid metabolism, regulation of the mitochondrial function, and aging. Given the potential role of the enzyme in several key metabolic processes, further research is required to fully characterize its substrate specificity and mechanism as well as its role in normal physiology and the significance of genetic polymorphisms in the development of pathological conditions, such as mitochondrial disease.

Acknowledgments—We are grateful to Anna Rast, Aurelia Weber, and Xiao-Ping Li for excellent technical assistance as well as Dr. Janina Tokarz for reading the manuscript. We also thank Dr. Margarita Ivanova for initial immunocytochemistry work and helpful discussions as well as Sabine Schmitt for expertise in the enrichment of mitochondria.

REFERENCES

1. Penning, T. M., and Drury, J. E. (2007) Human aldo-keto reductases: function, gene regulation, and single nucleotide polymorphisms. *Arch. Biochem. Biophys.* **464,** 241–250
2. Barski, O. A., Tipparaju, S. M., and Bhatnagar, A. (2008) The aldo-keto reductase superfamily and its role in drug metabolism and detoxification. *Drug Metab. Rev.* **40,** 553–624
3. Kondo, K. H., Kai, M. H., Setoguchi, Y., Eggertsen, G., Sjöblom, P., Setoguchi, T., Okuda, K. I., and Björkhem, I. (1994) Cloning and expression of cDNA of human δ4-3-oxosteroid 5β-reductase and substrate specificity of the expressed enzyme. *Eur. J. Biochem.* **219,** 357–363
4. Fujii, Y., Watanabe, K., Hayashi, H., Urade, Y., Kuramitsu, S., Kagamiyama, H., and Hayaishi, O. (1990) Purification and characterization of ρ-crystallin from Japanese common bullfrog lens. *J. Biol. Chem.* **265,** 9914–9923
5. Weng, J., Cao, Y., Moss, N., and Zhou, M. (2006) Modulation of voltage-dependent Shaker family potassium channels by an aldo-keto reductase. *J. Biol. Chem.* **281,** 15194–15200
6. Barski, O. A., Papusha, V. Z., Ivanova, M. M., Rudman, D. M., and Finegold, M. J. (2005) Developmental expression and function of aldehyde reductase in proximal tubules of the kidney. *Am. J. Physiol. Renal Physiol.* **289,** F200–F207
7. Penning, T. M. (2011) Human hydroxysteroid dehydrogenases and pre-receptor regulation: insights into inhibitor design and evaluation. *J. Steroid Biochem. Mol. Biol.* **125,** 46–56
8. Kabututu, Z., Manin, M., Pointud, J.-C., Maruyama, T., Nagata, N., Lambert, S., Lefrançois-Martinez, A.-M., Martinez, A., and Urade, Y. (2009) Prostaglandin F2α synthase activities of aldo-keto reductase 1B1, 1B3 and 1B7. *J. Biochem.* **145,** 161–168
9. Lemonde, H. A., Custard, E. J., Bouquet, J., Duran, M., Overmars, H., Scambler, P. J., and Clayton, P. T. (2003) Mutations in SRD5B1 (AKR1D1), the gene encoding δ(4)-3-oxosteroid 5β-reductase, in hepatitis and liver failure in infancy. *Gut* **52,** 1494–1499
10. Lyon, R. C., Johnston, S. M., Watson, D. G., McGarvie, G., and Ellis, E. M. (2007) Synthesis and catabolism of γ-hydroxybutyrate in SH-SY5Y human neuroblastoma cells: role of the aldo-keto reductase AKR7A2. *J. Biol. Chem.* **282,** 25986–25992
11. Srivastava, S., Chandra, A., Ansari, N. H., Srivastava, S. K., and Bhatnagar, A. (1998) Identification of cardiac oxidoreductase(s) involved in the metabolism of the lipid peroxidation-derived aldehyde-4-hydroxynonenal. *Biochem. J.* **329,** 469–475
12. Baba, S. P., Barski, O. A., Ahmed, Y., O'Toole, T. E., Conklin, D. J., Bhatnagar, A., and Srivastava, S. (2009) Reductive metabolism of AGE precursors: a metabolic route for preventing AGE accumulation in cardiovascular tissue. *Diabetes* **58,** 2486–2497
13. Guengerich, F. P., Cai, H., McMahon, M., Hayes, J. D., Sutter, T. R., Groopman, J. D., Deng, Z., and Harris, T. M. (2001) Reduction of aflatoxin B1 dialdehyde by rat and human aldo-keto reductases. *Chem. Res. Toxicol.* **14,** 727–737
14. Maser, E. (2004) Significance of reductases in the detoxification of the tobacco-specific carcinogen NNK. *Trends Pharmacol. Sci.* **25,** 235–237
15. Liu, S.-Q., Jin, H., Zacarias, A., Srivastava, S., and Bhatnagar, A. (2001) Binding of pyridine coenzymes to the β-subunit of the voltage sensitive potassium channels. *Chem. Biol. Interact.* **130,** 955–962
16. Malup, T. K., Kobzev, V. F., Zhdanova, L. G., Slobodianiuk, Si., and Sviridov, S. M. (2000) [Analysis of nucleotide sequences in a region of S100b protein gene in AKR/J, DBA/dJ and BALB/cLac mice]. *Mol. Biol. (Mosk.)* **34,** 366–367
17. Ramana, K. V. (2011) Aldose reductase: new insights for an old enzyme. *Biomol. Concepts* **2,** 103–114

18. Vikramadithyan, R. K., Hu, Y., Noh, H.-L., Liang, C.-P., Hallam, K., Tall, A. R., Ramasamy, R., and Goldberg, I. J. (2005) Human aldose reductase expression accelerates diabetic atherosclerosis in transgenic mice. *J. Clin. Invest.* **115,** 2434–2443
19. Gabbay, K. H. (2004) Aldose reductase inhibition in the treatment of diabetic neuropathy: where are we in 2004? *Curr. Diab. Rep.* **4,** 405–408
20. Dvornik, E., Simard-Duquesne, N., Krami, M., Sestanj, K., Gabbay, K. H., Kinoshita, J. H., Varma, S. D., and Merola, L. O. (1973) Polyol accumulation in galactosemic and diabetic rats: control by an aldose reductase inhibitor. *Science* **182,** 1146–1148
21. Kinoshita, J. H. (1990) A thirty year journey in the polyol pathway. *Exp. Eye Res.* **50,** 567–573
22. Bril, V., and Buchanan, R. A. (2006) Long-term effects of ranirestat (AS-3201) on peripheral nerve function in patients with diabetic sensorimotor polyneuropathy. *Diabetes Care* **29,** 68–72
23. Alexiou, P., Pegklidou, K., Chatzopoulou, M., Nicolaou, I., and Demopoulos, V. J. (2009) Aldose reductase enzyme and its implication to major health problems of the 21st century. *Curr. Med. Chem.* **16,** 734–752
24. Srivastava, S., Spite, M., Trent, J. O., West, M. B., Ahmed, Y., and Bhatnagar, A. (2004) Aldose reductase-catalyzed reduction of aldehyde phospholipids. *J. Biol. Chem.* **279,** 53395–53406
25. Vander Jagt, D. L., Robinson, B., Taylor, K. K., and Hunsaker, L. A. (1992) Reduction of trioses by NADPH-dependent aldo-keto reductases: aldose reductase, methylglyoxal, and diabetic complications. *J. Biol. Chem.* **267,** 4364–4369
26. Srivastava, S., Vladykovskaya, E., Barski, O. A., Spite, M., Kaiserova, K., Petrash, J. M., Chung, S. S., Hunt, G., Dawn, B., and Bhatnagar, A. (2009) Aldose reductase protects against early atherosclerotic lesion formation in apolipoprotein E-null mice. *Circ. Res.* **105,** 793–802
27. Shinmura, K., Bolli, R., Liu, S.-Q., Tang, X.-L., Kodani, E., Xuan, Y. T., Srivastava, S., and Bhatnagar, A. (2002) Aldose reductase is an obligatory mediator of the late phase of ischemic preconditioning. *Circ. Res.* **91,** 240–246
28. Ramana, K. V., Chandra, D., Srivastava, S., Bhatnagar, A., Aggarwal, B. B., and Srivastava, S. K. (2002) Aldose reductase mediates mitogenic signaling in vascular smooth muscle cells. *J. Biol. Chem.* **277,** 32063–32070
29. Cao, D., Fan, S. T., and Chung, S. S. M. (1998) Identification and characterization of a novel human aldose reductase-like gene. *J. Biol. Chem.* **273,** 11429–11435
30. Hyndman, D. J., and Flynn, T. G. (1998) Sequence and expression levels in human tissues of a new member of the aldo-keto reductase family. *Biochim. Biophys. Acta* **1399,** 198–202
31. Gallego, O., Belyaeva, O. V., Porté, S., Ruiz, F. X., Stetsenko, A. V., Shabrova, E. V., Kostereva, N. V., Farrés, J., Parés, X., and Kedishvili, N. Y. (2006) Comparative functional analysis of human medium-chain dehydrogenases, short-chain dehydrogenases/reductases and aldo-keto reductases with retinoids. *Biochem. J.* **399,** 101–109
32. Yoshitake, H., Takahashi, M., Ishikawa, H., Nojima, M., Iwanari, H., Watanabe, A., Aburatani, H., Yoshida, K., Ishi, K., Takamori, K., Ogawa, H., Hamakubo, T., Kodama, T., and Araki, Y. (2007) Aldo-keto reductase family 1, member B10 in uterine carcinomas: a potential risk factor of recurrence after surgical therapy in cervical cancer. *Int. J. Gynecol. Cancer* **17,** 1300–1306
33. Martin, H.-J., Breyer-Pfaff, U., Wsol, V., Venz, S., Block, S., and Maser, E. (2006) Purification and characterization of AKR1B10 from human liver: role in carbonyl reduction of xenobiotics. *Drug Metab. Dispos.* **34,** 464–470
34. Zhong, L., Shen, H., Huang, C., Jing, H., and Cao, D. (2011) AKR1B10 induces cell resistance to daunorubicin and idarubicin by reducing C13 ketonic group. *Toxicol. Appl. Pharmacol.* **255,** 40–47
35. Salabei, J. K., Li, X.-P., Petrash, J. M., Bhatnagar, A., and Barski, O. A. (2011) Functional expression of novel human and murine AKR1B genes. *Chem. Biol. Interact.* **191,** 177–184
36. Wabitsch, M., Brenner, R. E., Melzner, I., Braun, M., Möller, P., Heinze, E., Debatin, K. M., and Hauner, H. (2001) Characterization of a human preadipocyte cell strain with high capacity for adipose differentiation. *Int. J. Obes. Relat. Metab. Disord.* **25,** 8–15
37. Schmitt, S., Saathoff, F., Meissner, L., Schropp, E.-M., Lichtmannegger, J., Schulz, S., Eberhagen, C., Borchard, S., Aichler, M., Adamski, J., Plesnila, N., Rothenfusser, S., Kroemer, G., and Zischka, H. (2013) A semi-automated method for isolating functionally intact mitochondria from cultured cells and tissue biopsies. *Anal. Biochem.* **443,** 66–74
38. Mindnich, R., Haller, F., Halbach, F., Moeller, G., Hrabé de Angelis, M., and Adamski, J. (2005) Androgen metabolism via 17β-hydroxysteroid dehydrogenase type 3 in mammalian and non-mammalian vertebrates: comparison of the human and the zebrafish enzyme. *J. Mol. Endocrinol.* **35,** 305–316
39. Barski, O. A., Gabbay, K. H., Grimshaw, C. E., and Bohren, K. M. (1995) Mechanism of human aldehyde reductase: characterization of the active site pocket. *Biochemistry* **34,** 11264–11275
40. Bannai, H., Tamada, Y., Maruyama, O., Nakai, K., and Miyano, S. (2002) Extensive feature detection of N-terminal protein sorting signals. *Bioinformatics* **18,** 298–305
41. Barski, O. A., Mindnich, R., and Penning, T. M. (2013) Alternative splicing in the aldo-keto reductase superfamily: implications for protein nomenclature. *Chem. Biol. Interact.* **202,** 153–158
42. Wilson, D. K., Bohren, K. M., Gabbay, K. H., and Quiocho, F. A. (1992) An unlikely sugar substrate site in the 1.65 Å structure of the human aldose reductase holoenzyme implicated in diabetic complications. *Science* **257,** 81–84
43. Gallego, O., Ruiz, F. X., Ardèvol, A., Domínguez, M., Alvarez, R., de Lera, A. R., Rovira, C., Farrés, J., Fita, I., and Parés, X. (2007) Structural basis for the high all-*trans*-retinaldehyde reductase activity of the tumor marker AKR1B10. *Proc. Natl. Acad. Sci. U.S.A.* **104,** 20764–20769
44. McCormack, K., McCormack, T., Tanouye, M., Rudy, B., and Stühmer, W. (1995) Alternative splicing of the human Shaker K^+ channel β1 gene and functional expression of the β2 gene product. *FEBS Lett.* **370,** 32–36
45. Pongs, O., and Schwarz, J. R. (2010) Ancillary subunits associated with voltage-dependent K+ channels. *Physiol. Rev.* **90,** 755–796
46. Puranen, T. J., Poutanen, M. H., Peltoketo, H. E., Vihko, P. T., and Vihko, R. K. (1994) Site-directed mutagenesis of the putative active site of human 17β-hydroxysteroid dehydrogenase type 1. *Biochem. J.* **304,** 289–293
47. Byrns, M. C., Jin, Y., and Penning, T. M. (2011) Inhibitors of type 5 17β-hydroxysteroid dehydrogenase (AKR1C3): overview and structural insights. *J. Steroid Biochem. Mol. Biol.* **125,** 95–104
48. Luu-The, V., Tremblay, P., and Labrie, F. (2006) Characterization of type 12 17β-hydroxysteroid dehydrogenase, an isoform of type 3 17β-hydroxysteroid dehydrogenase responsible for estradiol formation in women. *Mol. Endocrinol.* **20,** 437–443
49. Endo, S., Matsunaga, T., Mamiya, H., Ohta, C., Soda, M., Kitade, Y., Tajima, K., Zhao, H.-T., El-Kabbani, O., and Hara, A. (2009) Kinetic studies of AKR1B10, human aldose reductase-like protein: endogenous substrates and inhibition by steroids. *Arch. Biochem. Biophys.* **487,** 1–9
50. Keller, B., Meier, M., and Adamski, J. (2009) Comparison of predicted and experimental subcellular localization of two putative rat steroid dehydrogenases from the short-chain dehydrogenase/reductase protein superfamily. *Mol. Cell. Endocrinol.* **301,** 43–46
51. Alías, M., Ayuso-Tejedor, S., Fernández-Recio, J., Cativiela, C., and Sancho, J. (2010) Helix propensities of conformationally restricted amino acids: non-natural substitutes for helix breaking proline and helix forming alanine. *Org. Biomol. Chem.* **8,** 788–792
52. Lam, C.-W., Yuen, Y.-P., Cheng, W.-F., Chan, Y.-W., and Tong, S.-F. (2006) Missense mutation Leu72Pro located on the carboxyl terminal amphipathic helix of apolipoprotein C-II causes familial chylomicronemia syndrome. *Clin. Chim. Acta* **364,** 256–259
53. Keenan, C., Ghaffar, S., Grant, A. W., Hinshelwood, A., Li, D., McGarvie, G., and Ellis, E. M. (2006) in *Enzymology and Molecular Biology of Carbonyl Metabolism*, Vol. 12 (Weiner, H., Plapp, B., Lindahl, R., and Maser, E., eds) pp. 388–395, Purdue University Press, West Lafayette, IN
54. Kelly, V. P., Sherratt, P. J., Crouch, D. H., and Hayes, J. D. (2002) Novel homodimeric and heterodimeric rat γ-hydroxybutyrate synthases that associate with the Golgi apparatus define a distinct subclass of aldo-keto reductase 7 family proteins. *Biochem. J.* **366,** 847–861
55. Mindnich, R., Möller, G., and Adamski, J. (2004) The role of 17β-hydroxysteroid dehydrogenases. *Mol. Cell. Endocrinol.* **218,** 7–20
56. Peltoketo, H., Luu-The, V., Simard, J., and Adamski, J. (1999) 17β-hydrox-

ysteroid dehydrogenase (HSD)/17-ketosteroid reductase (KSR) family: nomenclature and main characteristics of the 17HSD/KSR enzymes. *J. Mol. Endocrinol.* **23,** 1–11
57. Shafqat, N., Marschall, H.-U., Filling, C., Nordling, E., Wu, X.-Q., Björk, L., Thyberg, J., Mårtensson, E., Salim, S., Jörnvall, H., and Oppermann, U. (2003) Expanded substrate screenings of human and *Drosophila* type 10 17β-hydroxysteroid dehydrogenases (HSDs) reveal multiple specificities in bile acid and steroid hormone metabolism: characterization of multifunctional 3α/7α/7β/17β/20β/21-H. *Biochem. J.* **376,** 49–60
58. Clayton, P. T., Eaton, S., Aynsley-Green, A., Edginton, M., Hussain, K., Krywawych, S., Datta, V., Malingre, H. E. M., Berger, R., and van den Berg, I. E. T. (2001) Hyperinsulinism in short-chain L-3-hydroxyacyl-CoA dehydrogenase deficiency reveals the importance of β-oxidation in insulin secretion. *J. Clin. Invest.* **108,** 457–465
59. Heslegrave, A. J., and Hussain, K. (2013) Novel insights into fatty acid oxidation, amino acid metabolism, and insulin secretion from studying patients with loss of function mutations in 3-hydroxyacyl-CoA dehydrogenase. *J. Clin. Endocrinol. Metab.* **98,** 496–501
60. Schulz, N., Himmelbauer, H., Rath, M., van Weeghel, M., Houten, S., Kulik, W., Suhre, K., Scherneck, S., Vogel, H., Kluge, R., Wiedmer, P., Joost, H.-G., and Schürmann, A. (2011) Role of medium- and short-chain L-3-hydroxyacyl-CoA dehydrogenase in the regulation of body weight and thermogenesis. *Endocrinology* **152,** 4641–4651
61. Yang, S.-Y., He, X.-Y., and Schulz, H. (2005) 3-Hydroxyacyl-CoA dehydrogenase and short chain 3-hydroxyacyl-CoA dehydrogenase in human health and disease. *FEBS J.* **272,** 4874–4883
62. Miller, W. L., and Auchus, R. J. (2011) The molecular biology, biochemistry, and physiology of human steroidogenesis and its disorders. *Endocr. Rev.* **32,** 81–151
63. Yang, S.-H., Liu, R., Perez, E. J., Wen, Y., Stevens, S. M., Jr., Valencia, T., Brun-Zinkernagel, A.-M., Prokai, L., Will, Y., Dykens, J., Koulen, P., and Simpkins, J. W. (2004) Mitochondrial localization of estrogen receptor β. *Proc. Natl. Acad. Sci. U.S.A.* **101,** 4130–4135
64. Vasconsuelo, A., Milanesi, L., and Boland, R. (2013) Actions of 17β-estradiol and testosterone in the mitochondria and their implications in aging. *Ageing Res. Rev.* **12,** 907–917
65. Pedram, A., Razandi, M., Wallace, D. C., and Levin, E. R. (2006) Functional estrogen receptors in the mitochondria of breast cancer cells. *Mol. Biol. Cell* **17,** 2125–2137
66. Demonacos, C., Djordjevic-Markovic, R., Tsawdaroglou, N., and Sekeris, C. E. (1995) The mitochondrion as a primary site of action of glucocorticoids: the interaction of the glucocorticoid receptor with mitochondrial DNA sequences showing partial similarity to the nuclear glucocorticoid responsive elements. *J. Steroid Biochem. Mol. Biol.* **55,** 43–55
67. Demonacos, C. V., Karayanni, N., Hatzoglou, E., Tsiriyiotis, C., Spandidos, D. A., and Sekeris, C. E. (1996) Mitochondrial genes as sites of primary action of steroid hormones. *Steroids* **61,** 226–232
68. Yashin, A. I., Wu, D., Arbeev, K. G., and Ukraintseva, S. V (2010) Joint influence of small-effect genetic variants on human longevity. *Aging* **2,** 612–620
69. Witkowski, A., Joshi, A. K., and Smith, S. (2007) Coupling of the *de novo* fatty acid biosynthesis and lipoylation pathways in mammalian mitochondria. *J. Biol. Chem.* **282,** 14178–14185
70. Hiltunen, J. K., Schonauer, M. S., Autio, K. J., Mittelmeier, T. M., Kastaniotis, A. J., and Dieckmann, C. L. (2009) Mitochondrial fatty acid synthesis type II: more than just fatty acids. *J. Biol. Chem.* **284,** 9011–9015
71. Parl, A., Mitchell, S. L., Clay, H. B., Reiss, S., Li, Z., and Murdock, D. G. (2013) The mitochondrial fatty acid synthesis (mtFASII) pathway is capable of mediating nuclear-mitochondrial cross talk through the PPAR system of transcriptional activation. *Biochem. Biophys. Res. Commun.* **441,** 418–424
72. Schulte, U. (2001) Biogenesis of respiratory complex I. *J. Bioenerg. Biomembr.* **33,** 205–212
73. Calvo, S. E., Compton, A. G., Hershman, S. G., Lim, S. C., Lieber, D. S., Tucker, E. J., Laskowski, A., Garone, C., Liu, S., Jaffe, D. B., Christodoulou, J., Fletcher, J. M., Bruno, D. L., Goldblatt, J., Dimauro, S., Thorburn, D. R., and Mootha, V. K. (2012) Molecular diagnosis of infantile mitochondrial disease with targeted next-generation sequencing. *Sci. Transl. Med.* **4,** 118ra10